Analysis of Single Event Transients in Arbitrary Waveforms using Statistical Window Analysis

By

James L. Carpenter II

Daniel Loveless, PhD
Guerry Professor of Electrical
Engineering
(Committee Chair)

Donald R. Reising, PhD
UC Foundation Associate Pro-
fessor of Electrical Engineering
(Committee Member)

Raga Ahmed, PhD
Associate Professor of Electrical
Engineering
(Committee Member)

Analysis of Single Event Transients in Arbitrary Waveforms using Statistical Window Analysis

By

James L. Carpenter II

A Thesis Submitted to the Faculty of the University of Tennessee at Chattanooga in Partial
Fulfillment of the Requirements of the Degree of Master of Science: Engineering

The University of Tennessee at Chattanooga
Chattanooga, Tennessee

May, 2024

ABSTRACT

Window functions are commonly used in data processing to detect transient events or for time-averaging of frequency spectra. A generalized window function is demonstrated using the Ionizing Radiation Effects Spectroscopy (IRES) technique to enhance the measurement of transient anomalies within arbitrary waveforms. The IRES filter convolves time data with a sliding window consisting of a moment-generating function. The resulting time-dependent statistical moments are used to eliminate any steady-state signatures, including noise, and extract transient behaviors. The IRES filter analyzes data from heavy-ion exposures of commercial off-the-shelf (COTS) operational amplifiers, laser-induced transients in Complementary Metal-Oxide-Semiconductor (CMOS) phase-locked loops, and simulated transients in digital and analog circuits.The performance of the IRES filter in noisy environments shows that transients can be measured with higher fidelity than standard amplitude thresholding. This statistical window analysis technique may remove the need for complex triggering mechanisms on instrumentation and doesn't require a-priori knowledge of transient characteristics.

ACKNOWLEDGMENTS

TABLE OF CONTENTS

LIST OF TABLES

LIST OF FIGURES

ACKNOWLEDGEMENTS

CHAPTER 1

INTRODUCTION

An understanding of radiation effects in microelectronics is required for space-bound systems. The harsh space environment poses significant challenges for electronic systems due to ionizing radiation from solar emissions and Galactic Cosmic Rays (GCR). Single-event transients (SETs) are radiation-induced transients that can occur in electronic systems operating in space. Single-event transients (SETs) are radiation-induced temporal phenomena caused by the interactions of single ionizing particles that deposit energy in the electronic material, leading to a temporary or permanent malfunction. Before a mission, accelerated radiation testing of individual electronic components is typically carried out; testing at these radiation facilities is crucial to understand the effects of radiation on microelectronics and for developing radiation-hardened electronic systems capable of withstanding the harsh space environment.

In recent years, the commercialization of space has been on the rise, with private companies and governmental agencies launching satellites, space probes, and crewed spacecraft for communication, navigation, scientific exploration, and other applications at an increasing rate. The United States went from launching 190 objects into space in 2018 to launching 1,796 objects into space in 2022 [1]. However, with this increased commercialization, there has also been a higher demand for faster and more efficient ground-based radiation testing at facilities. Furthermore, commercial off-the-shelf (COTS) components, systems-on-chip (SOC), and heterogeneous packaged parts often require extra time, specialized facilities, and extensive preparation before experimentation, which can be a significant hurdle for researchers and companies. As a result, developing automation techniques for radiation testing, data collection, and analysis has become crucial to meet the growing constraints and demands for available time at heavy ion facilities.

1.1 Contributions to the State-of-the-Art

This work further investigates the uses of a non-invasive technique, Ionizing Radiation Effects Spectroscopy (IRES), for analyzing SETs in arbitrary signals and the ability to filter noise. Although this technique is simple, it could provide critical advantages during radiation testing. First, this technique uses a generalized window function to measure sudden changes caused by SETs in DC, RF, and Digital waveforms. The IRES filter produces time-dependent statistical moments by convolving time data with a sliding window that consists of a moment-generating function. These moments help to remove steady-state signatures, allowing for the extraction of the transient behaviors. Second, this work looks at the performance of the IRES filter for noisy environments such as heavy ion facilities and shows that transients could be measured with higher fidelity than standard instrumentation techniques, such as amplitude thresholding. This statistical window analysis technique may remove the need for complex triggering mechanisms on instrumentation and would not require *a-priori* knowledge of transient characteristics. The work presented in this thesis is demonstrated in the peer-reviewed paper [2].

1.2 Thesis Outline

The **Background** presents the fundamental knowledge needed to understand this work, the origins of IRES, single-event effects (SEE), and radiation testing.

The **Methods** present the new techniques developed in this study, including how IRES is used to analyze single-event effects, the generalized flow of the IRES model, and how the IRES window filter calculates the moments for the IRES spectrogram.

The **Results** present IRES's ability to analyze SET in various signals, beginning with the analog DC and RF signals, followed by the digital deterministic and stochastic signals, and concluding with a comparison between standard instrumentation amplitude thresholding and IRES filter with statistical thresholding while increasing the signal-to-noise ratio (SNR).

CHAPTER 2

BACKGROUND

2.1 Introduction

This section presents the relevant background information for the thesis. This section introduces the concept of single-event effects (SEE) caused by ionizing particles depositing charge to a device's sensitive nodes. SEE can lead to single-event transients (SETs) in analog systems (analog single-event transients or ASETs) and single-event upsets (SEUs) in digital electronic devices. SEE can result in temporary performance degradation or permanent damage, making them a critical concern for electronic systems used in space applications. Additionally, this section introduces the challenges associated with radiation testing, the limitations of conventional approaches, and the need for precise detection methods. Finally, the section covers the history of Ionizing Radiation Effect Spectroscopy (IRES) and its development for studying radiation effects. It also provides an overview of previous studies that used machine learning (ML) to analyze and classify the results of clock signals from an RF PLL circuit [3–5].

2.2 Space Environment

Space-bound electronic systems can experience many different radiation effects phenomena, such as Single Event Effects (SEE), Total Ionizing Dose (TID), and Displacement Damage Dose (DDD) during their mission life span. Ionizing radiation can penetrate spacecraft and affect the performance and reliability of electronic systems. This radiation originates from various sources, including the sun (solar particle events), galactic cosmic rays (GCR), and trapped radiation belts within Earth's Magnetosphere.

Trapped within the Earth's magnetosphere are the Van Allen belts. The inner belt is pri-
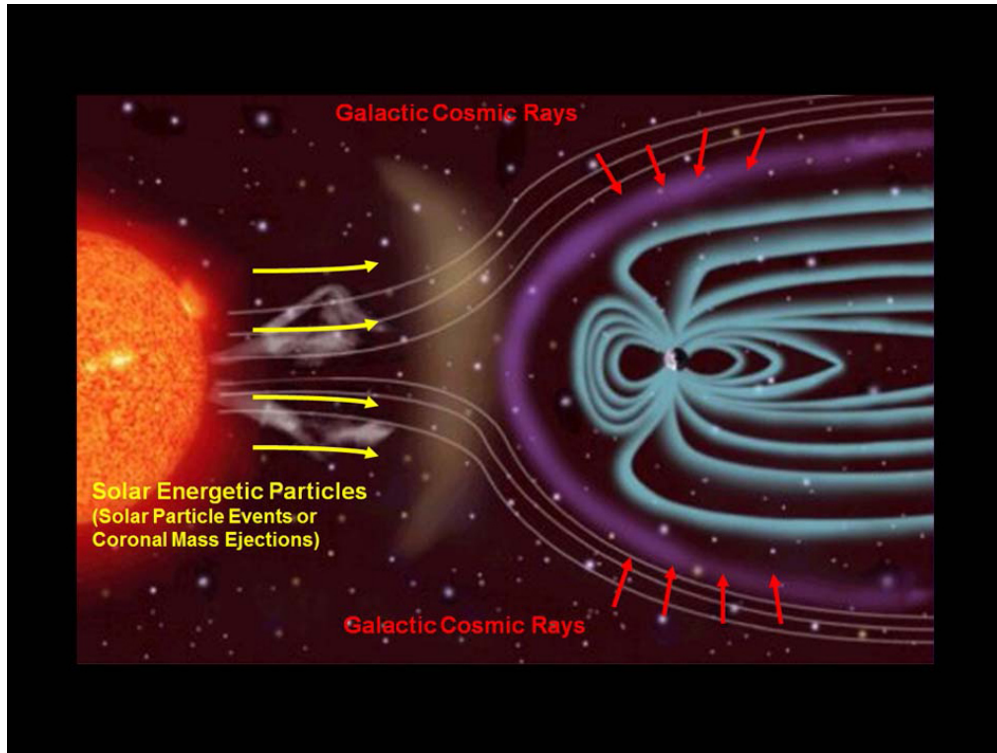
Figure 2.1   Sources of Ionizing Radiation in Interplanetary Space [6]

marily composed of high-energy protons, while the outer belt consists of a mixture of protons and electrons [7]. These particles are captured and held in place by the Earth's magnetic field, forming a protective barrier against incoming radiation from the solar wind and GCR shown in Fig. 2.1. However, the Van Allen belts can pose challenges for space missions, particularly for satellites and spacecraft that pass through these regions. Space agencies and mission designers must carefully consider the effects of space radiation and employ radiation-hardened designs and mitigation strategies to ensure the reliable operation of satellites and spacecraft. Making SEE a significant concern for space-based electronic systems and effective radiation testing analysis tools make IRES a necessity when studying the radiation effects in microelectronics.

2.3   Single-Event Effects

When a single ionizing particle collides with a sensitive node inside a semiconductor device, it causes an unwanted behavior called a Single Event Effect (SEE). This interaction causes

electron-hole pairs to form in the circuit's semiconductor material that can be collected at a metallurgical junction [8]. Linear Energy Transfer (LET) measures the energy deposited in a material by a charged particle per unit length of its path. LET depends on the type and energy of the particle, as well as the density and composition of the material it passes through. Shown in Fig. 2.2, is the process of charge generation and collection through drift and diffusion in a reverse-biased n+/p junction [9]. As the dimensions of semiconductor devices are decreasing with the technology trends, SEE is becoming more effective in disruption of the circuit operation [10]. SEE events can cause temporary performance degradation or permanent damage depending on the amount of charge deposited, circuit topology, and the amount of charge collected on the circuit node [10, 11]. SEE can be categorized as a Single Event Burnout (SEB), Single Event Functional Interrupt (SEFI), Single Event Transient (SET), and Single Event Upset (SEU) to name a few. This work is focused primarily on IRES detecting SET effects from the steady state.
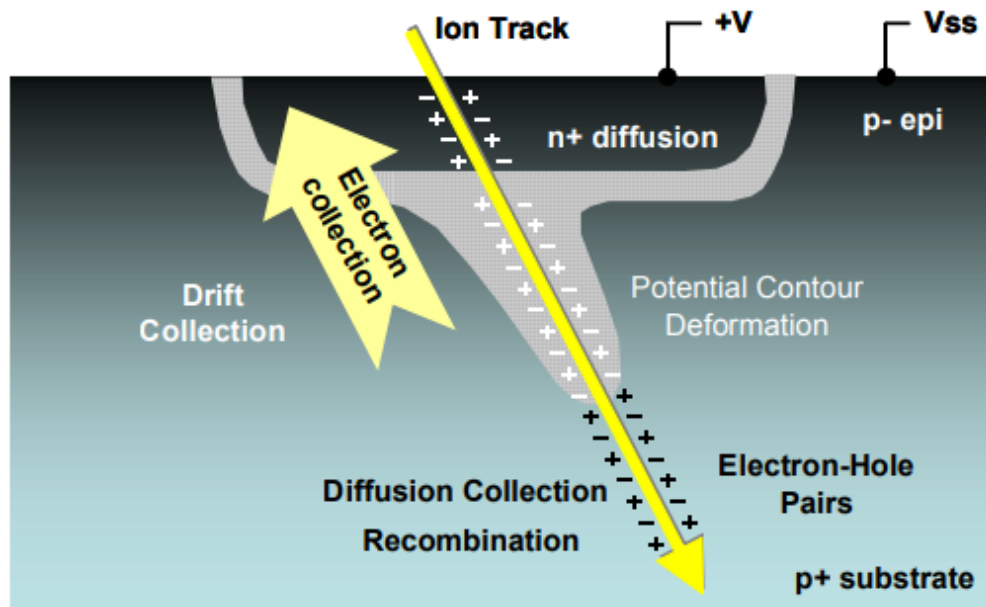
Figure 2.2   Illustration of an ion strike on a reverse-biased n+/p junction [9]

5

2.3.1 Digital Single Event Transients

If a particle strike happens in combinational logic, it can cause a voltage transient that changes the logic state at the affected node. These DSETs can lead to SEUs in memory cells if the timing exceeds latching requirements or if the total collected charge exceeds the cell's critical charge to upset. DSETs may propagate and induce an error in a memory element if the following three conditions are fulfilled [12–14]: 1) the SET is generated at a sensitive logic node, 2) as shown in Fig. 2.3 it propagates down an open logic path and arrives with sufficient amplitude and duration to change the memory state at a latch or other memory element, and 3) it arrives during the cell "window of vulnerability", i.e. when the clocking condition enables the transient capture as shown in Fig.2.4 [15]. Critical charge (Q_{crit}) is a metric used primarily for comparing SEE sensitivities of digital ICs [16]. Q_{crit} is the minimum amount of charge required for producing a SEE. Q_{crit} is a circuit property that may be calculated from the product of the node capacitance (C) and the minimum voltage excursion (ΔV) required for a SEE [17].
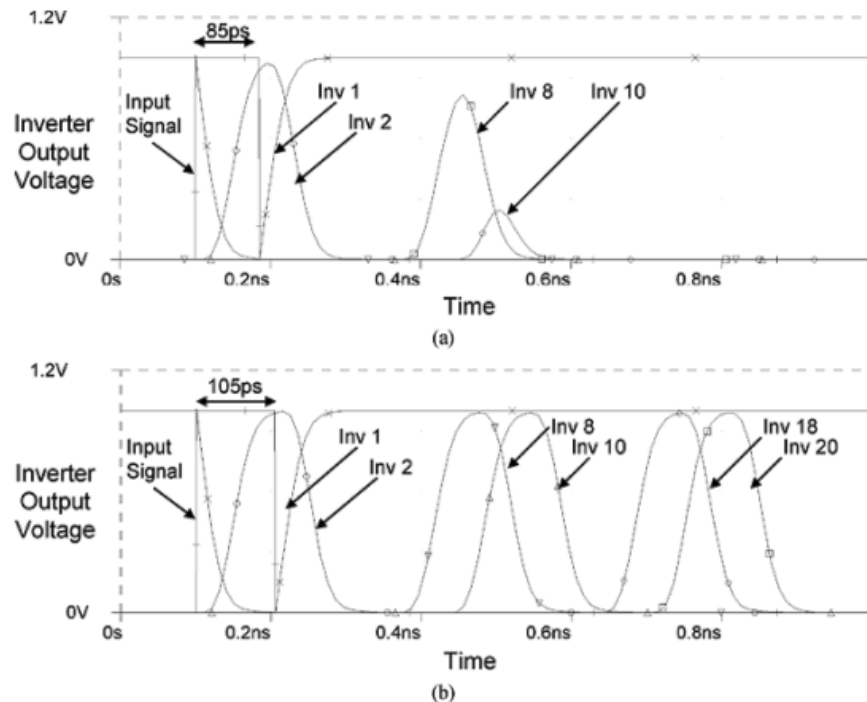
Figure 2.3 Examples of DSET pulses that (a) do not meet pulse width criteria to upset [18] and are electrically masked and (b) do meet criteria to upset [15]

6
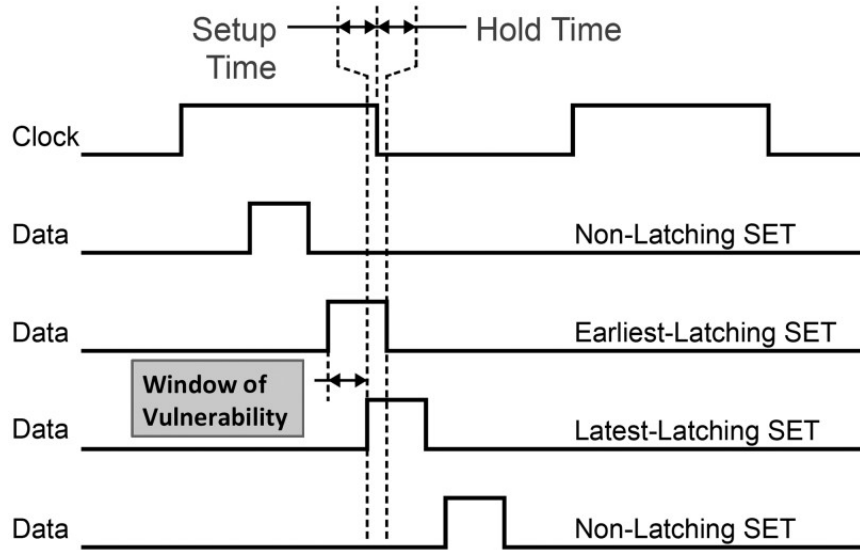
Figure 2.4   DSET latching window of vulnerability [19]

2.3.2   Analog Single Event Transients

When SETs are present in analog systems, they are called Analog Single Event Transients (ASETs). In a mixed-signal system, ASETs originating in the "analog" portion may become latched in a follow-on circuit; in the process, what starts as an ASET, ends up having characteristics of a digital upset [17]. Depending on the analog device ASETs can affect a device differently; for instance, operational amplifiers (OP-amp) like the LM124 can have positive, negative, and bipolar ASETs as shown in Fig. 2.5. In voltage compensators, ASETs exhibit variations solely in terms of their width and amplitude. For ASETs in pulse-width-modulators (PWMs), as shown in Fig. 2.6, having a shortened positive pulse for one of its cycles could also result in dropped pulses, shortened pulses, or phase shifts [20]. Finally, for a voltage-controlled oscillator (VCO) shown in Fig. 2.7, ASETs can affect the voltage amplitude and the desired oscillation frequency.

The value of Q_{crit} is somewhat arbitrary for linear devices since it must be related to a measurable quantity, such as ASET amplitude. Q_{crit} may be defined as the minimum amount of charge required to produce an ASET of a given amplitude in a particular operating configuration or with respect to a system application for which some minimum amount of charge must be collected to cause a system upset [17]. Many factors affect the ASET severity, including (a) ion strike location,

7

(a)

(b)

(c)

(d)
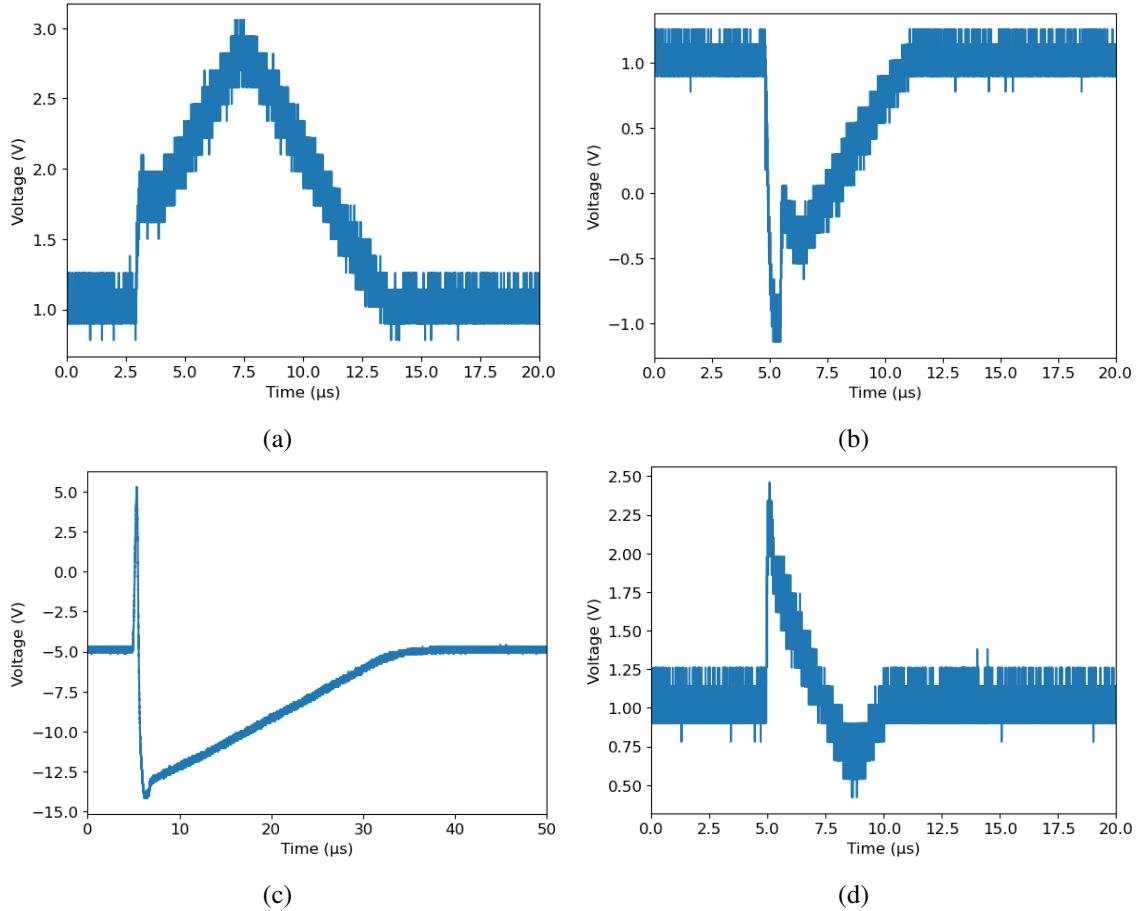
Figure 2.5   Analog SETs in the LM124 following exposure to Xe ions (16 MeV/amu) at the Lawrence
Berkeley National Laboratories (LBNL) 88" Cyclotron

(b) energy and nuclear charge of the incident ion, and (c) the device operating configuration (input voltage, output impedance, supply voltage, gain, etc.). Because the operating configuration determines ASET shape and sensitivity, measurements made for one operating configuration are not necessarily applicable to another [17]. Also, imperfections during the manufacturing process will lead to individual transistor responses from the other transistors in the same node. These variables have profound implications for testing, which must be performed for each operating configuration, making the process expensive and time-consuming [17].
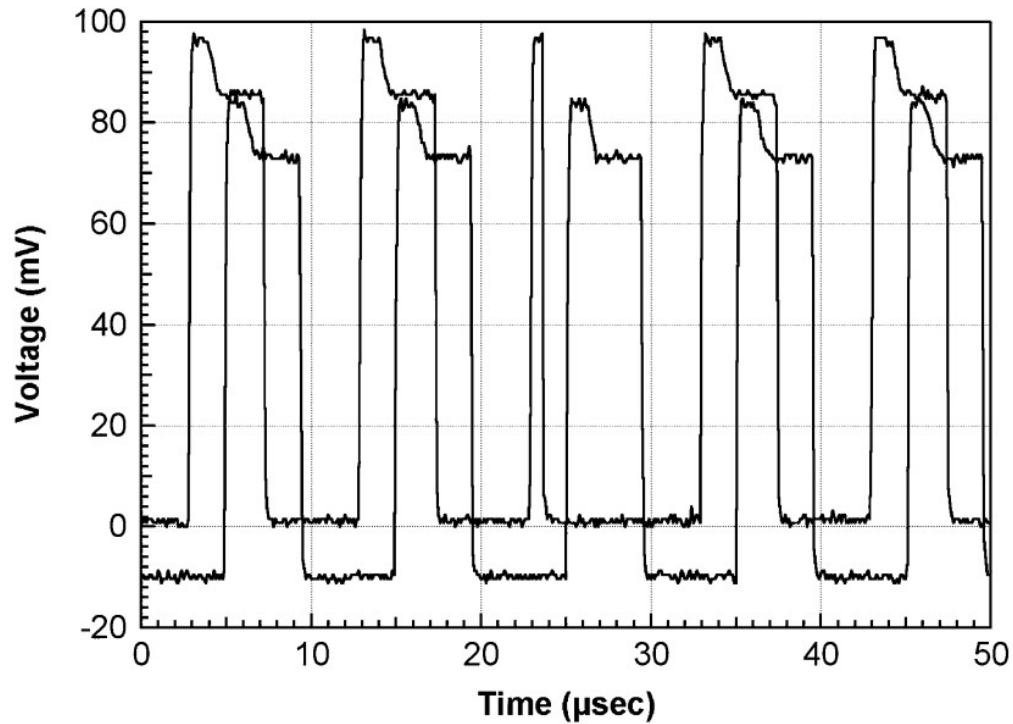
Figure 2.6   A pulse-width-modulator showing a shortened positive pulse in one of the pulse trains [21]

2.4   Radiation Testing

Typically, a test engineer will design an experiment to detect such anomalous behavior by determining a threshold error in voltage or current to trigger measurement hardware. This approach always presents a risk of missing unexpected erroneous behavior and is always based on the noise constraints imposed by the measurement system. Unfortunately, particle accelerators used in heavy ion irradiation are one way to test for SETs and often are extremely noisy environments in terms of injecting artificial noise into the system. Laser facilities are another way to test for SETs; although usually much less aggressive than a particle accelerator chamber in terms of the electromagnetic environment, some experiments can require specific attention on the signal integrity to minimize the impact of noise sources like scanning stages or optical modulators, and this is particularly the case for SET testing of analog and ultra-low power devices [23, 24]. Transients will not be detected if the SET effect occurs below the noise level set in the triggering hardware, which is often the case in RF signals shown in Fig. 2.8, where the red horizontal lines represent the instrument trigger to
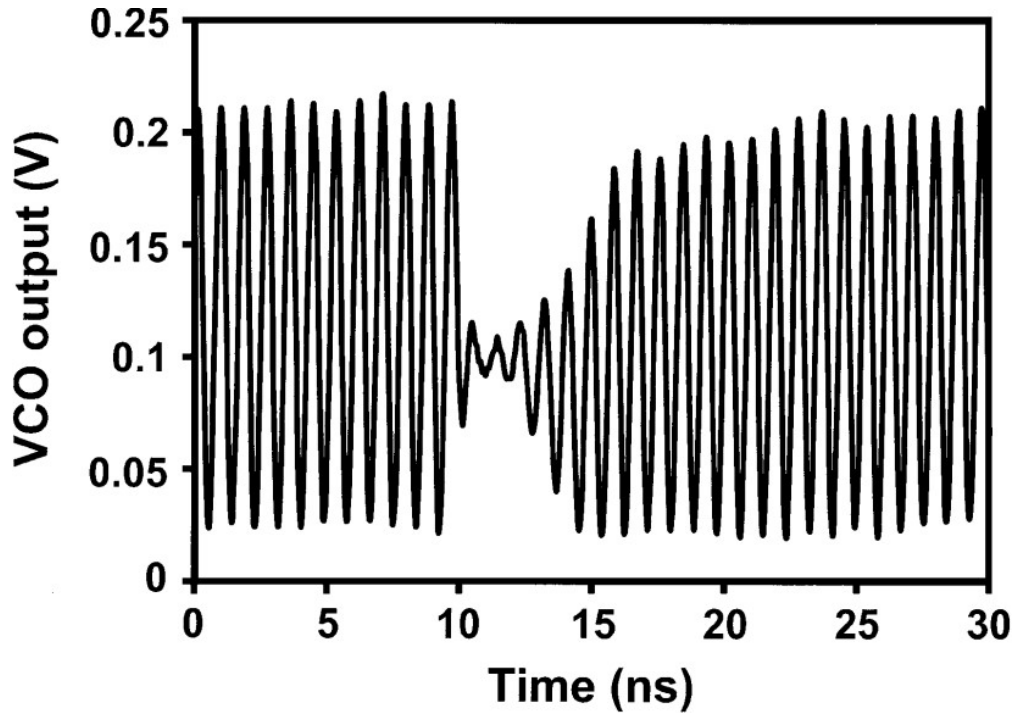
Figure 2.7   Output voltage as a function of time for a voltage-controlled oscillator The ASET appears as a
reduction in amplitude that lasts for about 10 cycles [22]

start recording the anomalous signal. So in the case of periodic signals, the start of the recording

process is usually done manually by the test engineer or an external trigger controlled by the start

and stop of a beam. This process leads to larger files that will take longer to analyze and may

not contain any SETs at that LET. This can lead to insufficient testing, wasting valuable time and

money.

2.4.1   Conventional Measurement Analysis

SEEs are identified by assessing a part's sensitivity to ion-stopping power, which is mea-

sured through its LET. LET refers to the energy loss per unit length as an ionizing particle travels

through a material. An SEE Cross-section is the device's relative sensitive area to ionizing radia-

tion and is a function of the number of errors n_{errors} and ion fluence $\Phi(x)$ at a LET x shown in Eq.

(2.1).
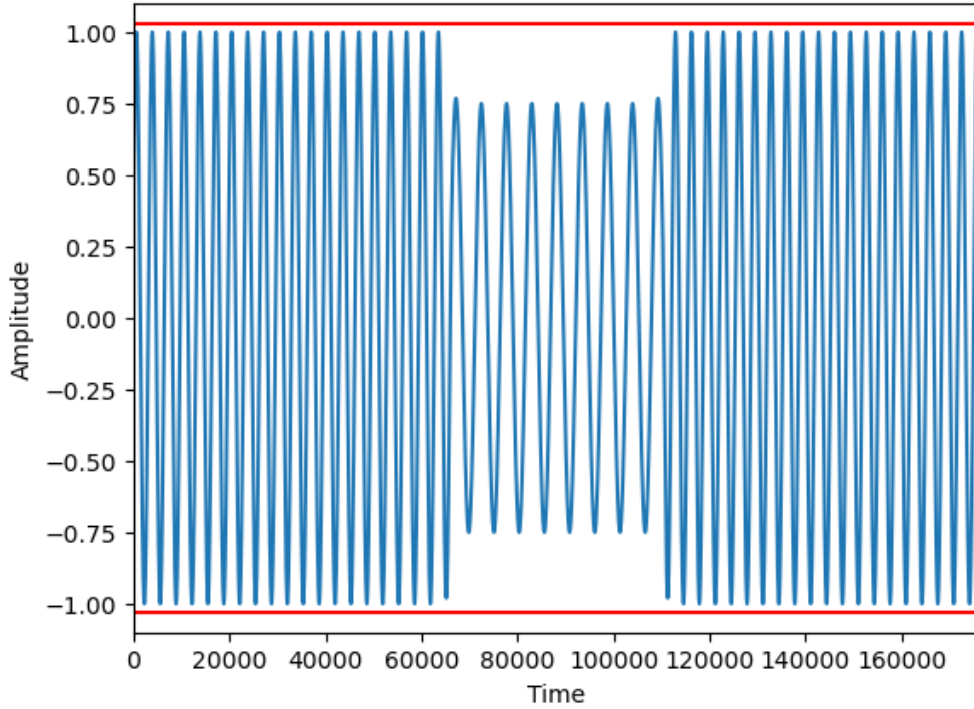
Figure 2.8 Example of an RF signal where the amplitude decreases before returning to its steady state where the red lines represent the trigger settings set on your instrument hardware

$$\sigma(x) = \frac{n_{errors}}{\Phi(x)} \tag{2.1}$$

When trying to understand a device's SET sensitivity, simply counting events and calculating a cross-section is not enough. To fully comprehend and develop a model of DSETs, only the width Δt is necessary. However, when it comes to ASETs and whether they pose a problem for amplifiers and compensators, both amplitude ΔV and width Δt are required. Combining knowledge of SET waveform signatures with modeling and simulation is the key to developing and evaluating potential techniques for mitigating SETs in complex circuits [15]. The details of the pulse shape are generally not necessary. However, it is essential to count only those SETs that exceed the minimum amplitude ΔV_{crit} and width Δt_{crit} values determined by the application for propagation through the system [17]. SETs, which manifest as unwanted signal transitions outside the minimum amplitude and width values, can be mitigated through hardware manipulation, such as

11

filtering or redundancy, at the cost of increased area and power and decreased bandwidth [8]. Regardless of the radiation-hardening-by-design (RHBD) technique used, all fundamentally involve a reduction in the amount of collected charge and/or the increase in the critical charge needed to generate a SET [20]. However, effective RHBD generally requires detailed knowledge of how the erroneous charge can change the observable behavior at the output of a device.

2.5   IRES Past Studies

Ionizing radiation effects spectroscopy (IRES) is based on Radio Frequency-Distinct Native Attributes (RF-DNA) fingerprinting methodologies and signal processing techniques [25–35]. RF-DNA is used in wireless communication applications to augment security protocols by basing authenticity requirements on statistical features derived from transmitted waveforms. Features are associated with intrinsic variability within the system and are often measured via short-time domain statistical behavior. These inherent variabilities within the system act as unique identifiers similar to how a fingerprint is a unique feature for the identification of an individual.

The first publication of the IRES method for monitoring devices for radiation effects analysis looked at total ionizing dose (TID) degradation [3]. It used IRES and a 2-D linear discriminant (LD) machine learning classification model in the 130-nm CMOS phase-locked-loop (PLL) and voltage-controlled oscillator (VCO) to predict TID levels based on a given bias voltage. By utilizing IRES's mean and standard deviation features of the instantaneous frequency, TID levels can be classified at a given bias voltage. The IRES-ML combination was able to predict TID levels and bias voltage with an impressive accuracy rate of between 97.5% and 100%. The prediction accuracy remained high for training set sizes of 50 samples or greater but decreased to 96.47% and 94.95% for training set sizes of 40 and 30 samples, respectively [3]. These were the first results, demonstrating the potential of IRES in device monitoring for radiation effects analysis.

The next two publications of the IRES method for monitoring devices for radiation effects analysis looked at single event transients (SETs) in the 130-nm CMOS PLL [4,5]. In these studies, the k-nearest neighbors (kNNs) ML algorithm was used with IRES data. The statistical features,

12

derived from several standard circuit metrics like cycle-to-mean (c2m), cycle-to-cycle (c2c), and frequency (f) and up to eight moment-generating functions, show that SETs can be automatically identified by the kNN models, with several features resulting in greater than 98% correct identification of SETs [5]. These results further demonstrate the potential of IRES method in device monitoring for radiation effects analysis but now also for SETs.

Thus far, previous works introduced IRES for *in-situ* analysis of TID degradation [3] and SETs in RF circuits [4, 5]. IRES leverages time-frequency domain analysis techniques common in data communications [36, 37] for identifying anomalous behavior by "imaging" the statistical features of a waveform. However, all previous studies that leverage IRES use in clock signals from an RF PLL circuit [3–5]. Additionally, these studies all paired IRES with machine learning (ML) for the study and classification of the results.

2.6 Summary

In this section, the relevant background information was discussed and one of particular interest was the detection of SET effects, which can lead to voltage transients and changes in logic states. These Digital Single Event Transients (DSETs) and Analog Single Event Transients (ASETs) have significant impacts on various circuit elements including memory cells, operational amplifiers, comparators, pulse-width modulators, and voltage-controlled oscillators. To test for such effects, radiation testing methods involving particle accelerators and laser facilities are employed, albeit with challenges related to noise and maintaining signal integrity. Conventional measurement analysis and radiation-hardening-by-design techniques are utilized to mitigate the impact of SEE. One promising approach is Ionizing Radiation Effects Spectroscopy (IRES), which leverages RF-DNA fingerprinting and machine learning to monitor devices for radiation effects analysis. Previous studies have demonstrated the potential of IRES in detecting total ionizing dose (TID) degradation and analyzing SETs in PLL CMOS circuits. In the next chapter, we will look at how IRES detects SET signatures in arbitrary signals and the experimental setups for each device under test.

CHAPTER 3

METHODOLOGY

3.1   Introduction

Ionizing Radiation Effects Spectroscopy (IRES) offers a powerful and versatile methodology for characterizing the effects of ionizing radiation on electronic devices and systems. By leveraging statistical profiles and moment-based analysis, IRES enables the detection and assessment of transient behavior, including SETs, in an efficient and reliable manner. This technique enhances measurement fidelity, particularly in noisy environments, and contributes to the development of radiation-hardened technologies. In the following sections, we will delve deeper into the working principles and advantages of IRES, providing insights into its application in radiation testing and analysis.

3.2   IRES Window Filter

IRES extracts stochastic features of a waveform and uses the resulting profiles for a statistics-based assessment of transient behavior. The presence of a transient is determined based on the likelihood that a sampled behavior is statistically different from expected steady-state behavior.

A diagram of the general methodology is shown in Fig. 3.1 [2], where an arbitrary discrete time-domain waveform or data sequence is analyzed by viewing smaller "windowed" segments and sliding the viewing window throughout the waveform. This work uses a window function for computing the statistical moments to develop time-dependent statistical profiles. The window function can include features from any signal metric in the time or frequency domain. Furthermore, the window function may be applied concurrently or sequentially with additional windowing functions.

14
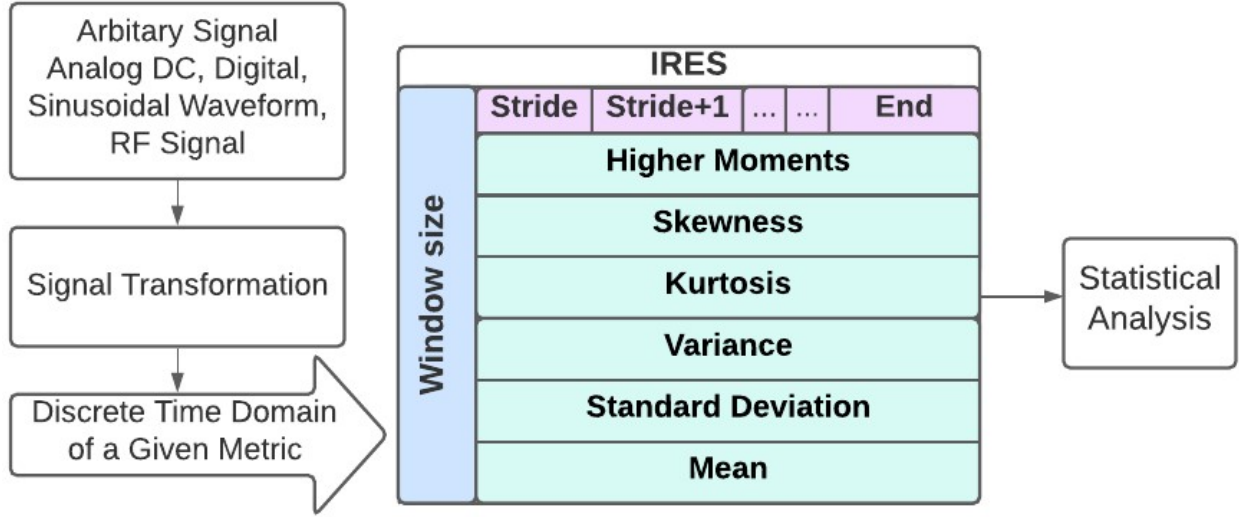
Figure 3.1   Block diagram of the IRES methodology where an arbitrary time-domain waveform or data sequence is analyzed by viewing smaller "windowed" segments and sliding the viewing window throughout the waveform. A statistical profile is developed with respect to time and can include features from any signal metric in the time or frequency domain [2]

The proposed IRES window filter convolves measured data with a statistical moment-generating function through a sliding window. As a result, any number of statistical moments describing nuanced features of data contained within a given window can be computed. Given time-domain data within a window, represented as a random variable X, the kth moment of a random variable X is defined as the expectation of X^k, or $E(X^k)$. Likewise, the kth central moment of a random variable X is defined to be $E((X - E(X))^k)$. For example, the first moment can be computed by determining the expectation of X and is defined as the mean (μ), whereas the second central moment is defined as the variance (σ^2). Rather than deriving expressions for the individual moments, a moment-generating function, M_{X_i}, can compute all moments of X. Eq. (3.1) represents the moment generating function for X_i, the data consisting of the N time samples within the ith window and consisting of real-valued numbers t. In other words, M is determined as the expectation of the random variable e^{tX_i}.

$$M_{X_i}(t) = E(e^{tX_i}) \tag{3.1}$$

For a discrete and windowed data set, M can be reduced to (3.2), where $P_i(x)$ is the probability mass function (PMF) of X_i.

$$M_{X_i}(t) = \sum_{X_i} e^{tx} P_i(x) \tag{3.2}$$

It follows that M can then be used to derive up to k moments of X_i using (3.3), where the kth derivative of M with respect to t is computed and evaluated at $t = 0$. Thus, any number of moments $E(X^k)$ can be calculated within each discrete window and appended to form an IRES spectrogram as described in [4].

$$E(X^k) = \left. \frac{d^k}{dt^k} M_{X_i}(t) \right|_{t=0} \tag{3.3}$$

The first four moments (*i.e.,* mean μ, variance σ^2, skewness γ, and kurtosis κ) are described in [4]. μ is useful for identifying the worst-case deviation of the signal, whereas σ^2 or σ measures emphasize the sharpness of a transition within the signal. γ and κ are measures indicating an abrupt transition from steady-state (*i.e.*, the start, recovery, or ending of a transient anomaly). Here, the 6th and 7th moments are also used, representing smoothed versions of γ and κ, respectively. The 6th and 7th moments may be used to identify an anomaly through more discrete indicators of a disruption.

An advantage of the IRES moment-generating filter is the ability to process arbitrary (*i.e.*, the signal type is irrelevant) discrete waveforms. The resulting statistical moments can aid in detecting abnormalities caused by SETs, improving measurement fidelity, especially in noisy environments. An example is shown in Fig. 3.2, where time-sequenced moments of a clock signal's frequency and phase are used to develop and visualize the shifting statistical profiles before, during, and after the presence of a SET. In Fig. 3.2, a clock signal's behavior (a) pre-, (b) during, and (c) post-strike are visualized after applying IRES window filters and normalizing each moment to the maximum value in each field. PMFs are estimated within the sliding windows, and several statistical moments are calculated. Here, the time evolution of the mean of the signal's frequency

16
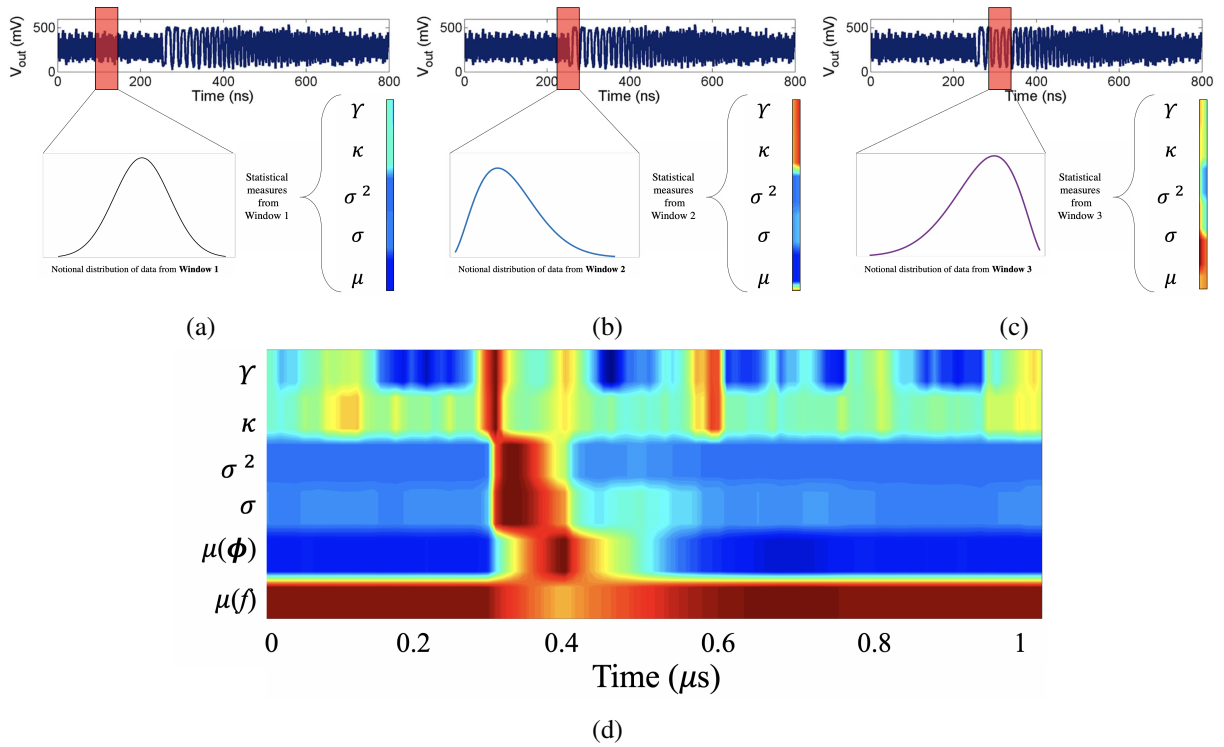
Figure 3.2   Example IRES spectrogram for visualizing various statistical moments of a signal's behavior (a) pre-, (b) during, and (c) post-strike. Probability density functions are estimated within the sliding windows, and several statistical moments are calculated. Here, the time evolution of the mean of the signal's frequency ($\mu(f)$), the mean of the signal's phase ($\mu(\phi)$), the variance (σ^2), standard deviation (σ), kurtosis (κ) and skewness (γ) of the phase are illustrated. after [5]

($\mu(f)$), the mean of the signal's phase ($\mu(\phi)$), and σ^2, σ, κ and γ of the phase are illustrated following a perturbation by an ion [5].

3.2.1   IRES Window Size

To optimize window size, the aim is to minimize the impact of the signal's steady state portion allowing for the extraction of the SET. This is particularly useful for periodic signals in which identifying the SET is sometimes challenging. IRES significantly decreases the AC portion, leaving only the DC SET. To ensure accurate features of SET signal, the window size should be kept small. The ideal window size for periodic signals is determined by calculating the period T of the periodic signal using eq. (3.4), where f represents frequency.

$$T = \frac{1}{f} \tag{3.4}$$

(a)

(b)
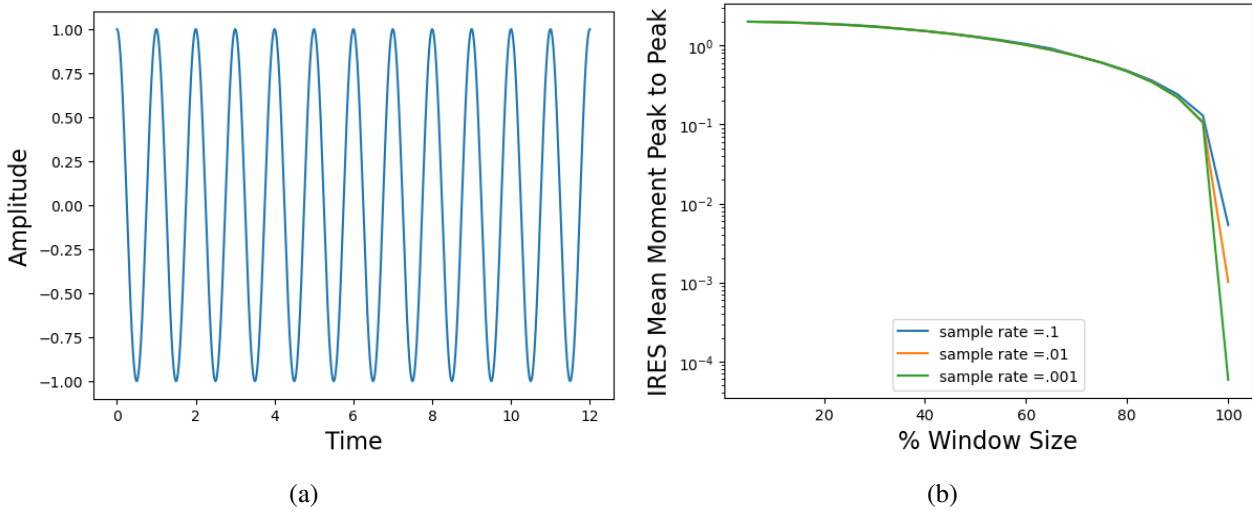
Figure 3.3   (a) represents a typical periodic sinusoidal signal having an amplitude of 1. Three different sample rates from signal (a) were compared in Fig. (b) demonstrating the relationship of setting the window size as a percent of the (a) sinusoidal signal's period to the peak-to-peak amplitude of IRES's mean moments

As shown in Fig. 3.3 (b) by setting the window size to the period it standardizes the values inside the window to have very little to no variations of the statistical moments as the window moves along the periodic signal. Also, inferred by Fig. 3.3 (b) if the frequency of the signal was to change so that the window would not fall on the optimum window size it would show up as an increase in amplitude shift in the IRES moments. As the number of samples per cycle increases the amplitude of the signal decrease allowing for smaller variations to be detected.

3.2.2   IRES Statistical Threshold

When radiation testing, certain devices can experience gradual shifts in their normally de-signed steady-state operating conditions. This effect is called total ionizing dose (TID). The TID effect causes issues for modern SET studies because the test engineer will design an experiment to detect SET anomalous behavior by determining a threshold error in voltage or current to trigger measurement hardware. If the threshold error in voltage or current changes throughout the test

due to TID, it will cause the test engineer also to change the trigger setting on the measurement hardware. IRES allows for a statistical threshold to be implemented without the need to redefine the error threshold due to the TID effect. The IRES statistical threshold is computed by taking the mode of the mean moment (μ) plus or minus (due to SETs being bi-directional) mode of the standard deviation moment (σ) as shown in Eq. (3.5).

$$IRES_{thresh} = mode(\mu) \pm mode(\sigma) \tag{3.5}$$

The effectiveness of Eq. 3.5 takes advantage of the nature of a transient, being a short anomalous behavior, meaning the most frequent value (mode) of a signal should be the steady state. IRES's (μ) moment, which can be thought of as a filter version of the raw signal, amplifies the SET signature from the steady-state signature. IRES also builds a series of discrete times of the standard deviation moment σ of the signal. Since signals are affected by added environmental noise the standard deviation moment is selected over the variance moment for that reason. With the addition of a binary conditional statement the extraction of the SET duration is possible with Eq. (3.6),

$$f(x,y) = \begin{cases} 1 & \text{if } f(x,y) < lower\ IRES_{thresh}\ \text{OR}\ f(x,y) > upper\ IRES_{thresh} \\ 0 & otherwise \end{cases} \tag{3.6}$$

where signal values below the $lowerIRES_{tresh}$ and above $upperIRES_{tresh}$ are assigned a binary value of 1 meaning that part of the signal lies outside the signal steady state parameter. IRES's process of extracting the SET is shown in Fig. 3.4. One assumption is that the instigating window is large enough for the most frequent value of the μ moment. It needs to be the nominal steady-state value and not part of the SET signature as shown in Fig. 3.4 (e). Where the $lower\ IRES_{thresh}$ and $upper\ IRES_{thresh}$ are placed on the saturation part of the SET.
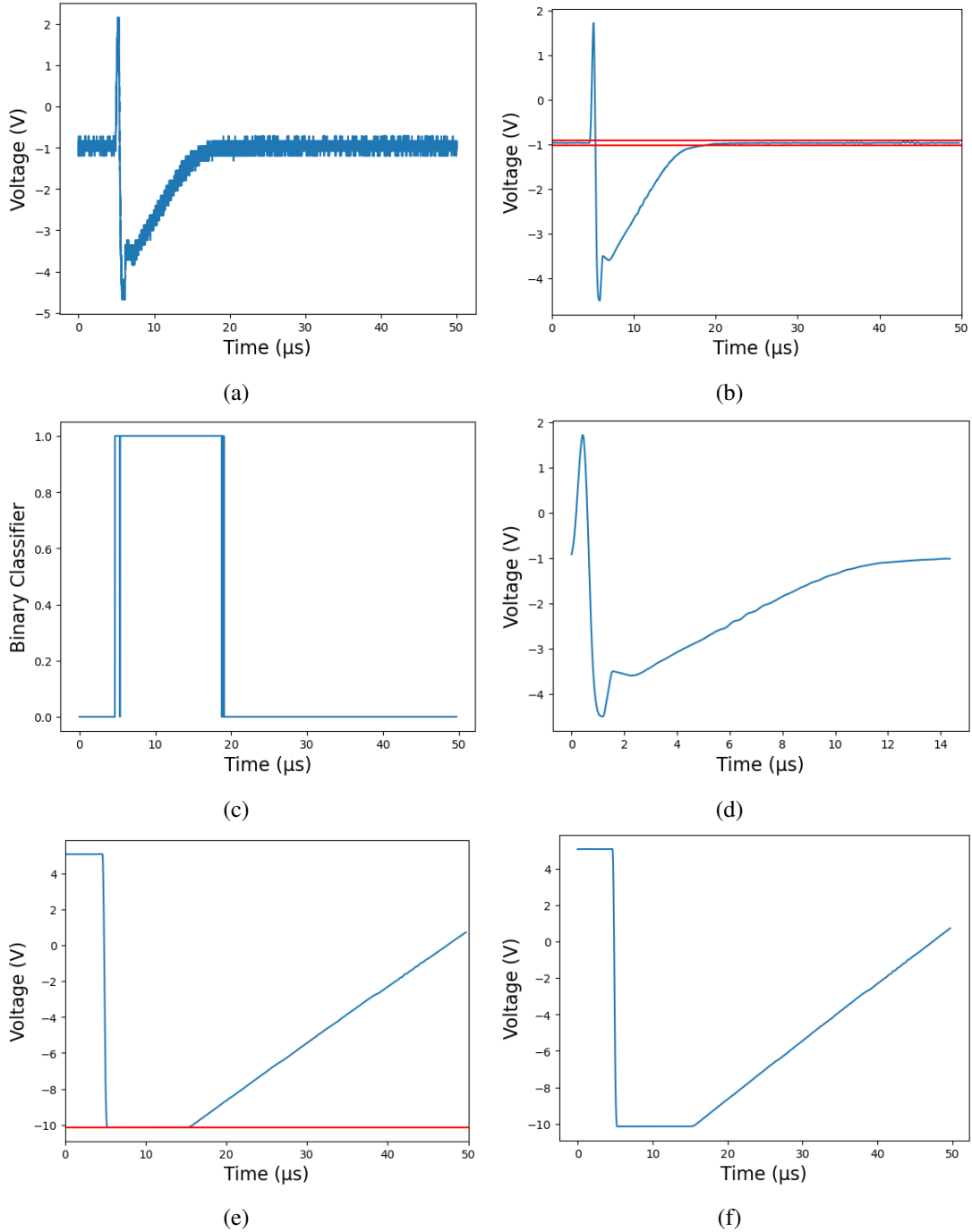
Figure 3.4 Raw signal (a) is an ASET collected in the LM124 while at LBNL. Fig. (b) and (e) the output of IRES's mean moment in blue and in red the results of $IRES_{thresh}$. (c) being the results of the binary conditional statement where the values equal to 1 fall outside the nominal steady state indicating a SET. Finally, Fig. (d) and (f) show the full width of the extracted SET

3.3   Device Under Test

3.3.1   Device Under Test LM124

The LM124 Op-Amps were irradiated at the LBNL 88" Cyclotron and the MSU FRIB linear accelerator. At LBNL, Xe and Kr ions in the 16 MeV/amu cocktail were utilized in air (with approximate LET values of 49 MeV*cm^2/mg and 25 MeV*cm^2/mg, respectively) with fluxes ranging from 4.5e3 to 2.0e7 ions/cm^2/s. At the MSU FRIB, 20 MeV/amu Ar and 30.5 MeV/amu O ions were utilized (with approximate LET values of 7.9 MeV*-cm^2/mg and 1.0 MeV*cm^2/mg, respectively) with fluxes ranging from 4.5e3 to 1e4 ions/cm^2/s. SRIM [38] was used in all cases to determine the LET at the surface of the de-lidded die.
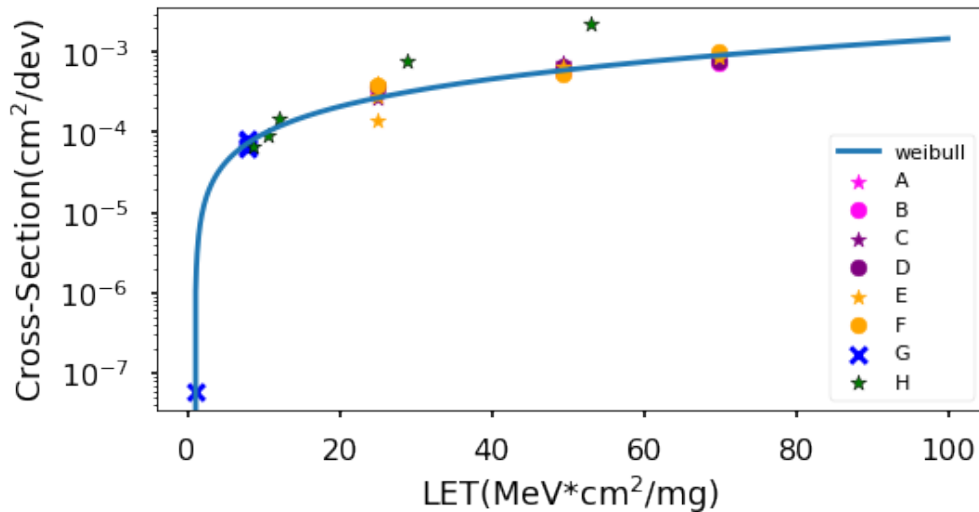
Figure 3.5   LM124 SET cross-section (cm^2/dev) versus LET (MeV*cm^2/mg) for data obtained at LBNL and MSU and compared to the reference data "H" represented by green stars obtained at NSRL [20]. TABLE 3.1 details the test configurations [2]

The LM124 DUTs were tested in inverting and non-inverting configurations having different gains, varying input voltages, and with V_{DD} = 15 V and V_{SS} = -15 V. TABLE 3.1 details the configurations of each DUT. The angle of incidence was set to either 0 or 45 degrees. Each ion exposure was conducted until 100 SETs were acquired, except for the O ion at the FRIB that was run to a total fluence of 5.16e7 ions/cm^2. In this case, the incident LET (of approximately 1 MeV*cm^2/mg) was near the LET threshold of the LM124, and the fluence was chosen to estab-

Table 3.1   Testing conditions

Measurements	Device	Facilities	Configuration	Gain	Bias
A	LM124	LBNL	Inverting	10V/V	0.1V
B	LM124	LBNL	Inverting	10V/V	0.5V
C	LM124	LBNL	Non-Inverting	10V/V	0.1V
D	LM124	LBNL	Non-Inverting	10V/V	0.5V
E	LM124	LBNL	Non-Inverting	1V/V	1V
F	LM124	LBNL	Non-Inverting	1V/V	5V
G	LM124	FRIB(MSU)	Non-Inverting	1V/V	1V
H	LM124	NASA	Non-Inverting	1V/V	1V
I	Mixed-Signal PLL*	NRL			

* The mixed-signal PLL circuit, fabricated in the IBM 130 nm CMRF8RF CMOS technology, is detailed in [39]. The device has a center frequency of 200 MHz and a maximum frequency of 530 MHz. The locking range of the PLL is between 40 and 350 MHz, with a gain of 7.75 GHz/V.

lish a limiting cross-section; three SETs were recorded.

The LM124 DUTs were connected to a Tektronix DPO7104 Oscilloscope (Oscope) through coaxial cables and BNC connectors. A window trigger was set to be ± 0.5 V above the nominal output voltage, and pre-irradiation measurements were obtained to ensure that no false-positive, noise-induced events were captured. SETs were saved locally to a solid-state drive. A programmable DC power supply was connected by a coaxial cable and a BNC connector to the differential input of the DUT. A second power unit supplied a biasing voltage of ± 15 V. The programmable DC power supply and Oscope were connected to a computer through an ethernet switch. Python script commands were sent from the computer to the testing equipment. After testing, the SET data were evaluated with the IRES analysis software. Fig. 3.5 [2] shows the SET cross-section (cm^2/dev) versus LET (MeV*cm^2/mg) results for the LM124 DUTs irradiated at LBNL and MSU. Data obtained at NSRL from [20], marked by the green stars in Fig. 3.5 [2], are also included for reference and to show consistent results with prior literature. A Weibull curve was used to fit the LM124's measured cross-section probability data to a particle LET. The Weibull curve is a four-parameter best fit to the data, calculating the rate of radiation-induced single event effects for a device using

Eq. (3.7).

$$F(x) = A(1 - e^{-\frac{(x-x_o)^s}{W}})$$

(3.7)

Where x is the effective LET in (MeV-cm^2/mg), $F(x)$ is the SEE cross-section (cm^2/dev), A is the saturating cross-section, x_o is the onset parameter, W is the width parameter, and s is the dimensionless exponent. The Weibull curve shown in Fig. 3.5 had the following fitting parameters $A = 1.47e-3$, $x_0 = 1.01$, $W = 60$, and $s = .42$.

3.3.2 Device Under Test CMOS PLL
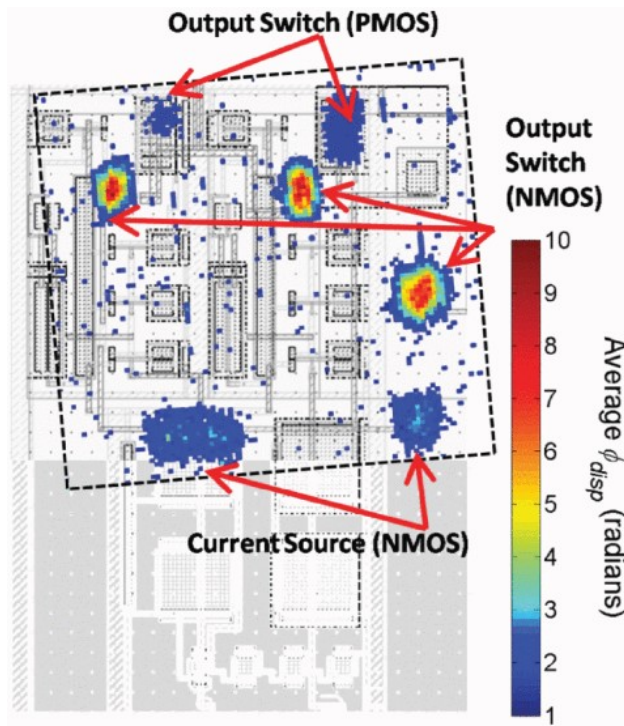
Figure 3.6   2-D spatial map of the regions in the CP subcircuit sensitive to SETs. The experiment was performed using laser TPA at a step size of 0.2 μm. Each pixel represents the average maximum phase displacement (instantaneous cycle-to-cycle phase error) for ten SETs generated at each x -y location. The image shows that the output of the CP circuit, in particular, the nMOS switches and current sources contain the most sensitive junctions due to their ability to deplete the charge stored in CLPF (after [39])

A custom PLL fabricated in a 130 nm CMOS technology was used to obtain transient data at NRL's TPA facility using a high peak power femtosecond laser at sub-bandgap optical wave-

lengths [40–44]. The DUT was mounted on a motorized *xyz* translation platform with 0.1 μm resolution, and the TPA laser was focused on the PLL's sub-circuits. Waveforms were collected at the PLL circuit's output at the resulting ten thousand (10,000) strike locations, allowing for visualization of the 2-D spatial sensitivity map shown in Fig. 3.6. Ten independent measurements were taken at each strike location, amounting to one hundred thousand (100,000) individual waveforms. Additional details on this data set can be found in [5,39]. This work leverages these data to analyze the effectiveness of the IRES window filter on sinusoidal data in the presence of noise.

3.4 Summary

Ionizing Radiation Effects Spectroscopy (IRES) is a powerful technique that enables the characterization of ionizing radiation effects in devices and systems. By extracting features of a waveform and analyzing statistical profiles, IRES allows for a thorough assessment of transient behavior. The windowed analysis of time-domain waveforms, where statistical moments are computed using a moment-generating function. These moments provide valuable information about the waveform, such as mean, variance, skewness, and kurtosis. The IRES technique offers several advantages, including its ability to process arbitrary waveforms and its effectiveness in detecting anomalies caused by Single Event Transients (SETs). It also addresses challenges posed by Total Ionizing Dose (TID) effects by implementing a statistical threshold that remains consistent throughout the test. The optimal window size is determined based on the periodic signal's period, minimizing the impact of steady-state portions and facilitating SET extraction. Overall, IRES contributes to improving measurement fidelity, particularly in noisy environments, and enables a comprehensive analysis of ionizing radiation effects on devices.

CHAPTER 4

RESULTS

4.1   Introduction

This section presents the results from simulations and measured data collected on an LM124 at LBNL and Michigan State University (MSU) FRIB facility. This section goes over the findings to analyze SET in various signals. It begins with an analysis of analog DC and RF signals, followed by an analysis of digital deterministic and stochastic signals, and concludes with a comparison between standard instrumentation amplitude thresholding and IRES filtering with statistical thresholding in the presence of noise. Any erroneous behavior can be identified *in-situ*, allowing for further analysis by a radiation test engineer or through ML.

4.2   IRES for Analog Signals

Figs. 4.1(a) and (c) illustrate examples of analog SETs captured from an LM124 during a heavy ion radiation test at LBNL. In both cases, the LM124 was configured in a non-inverting, unity-gain configuration (*i.e.*, voltage follower) with a DC input of 1 V. The Xe ion (16 MeV/amu) was utilized with an incident LET of 49.3 MeV*cm^2/mg. Fig. 4.1(e) illustrates a similar transient with a sinusoidal input where the DC offset was 1 V, and the sinusoidal amplitude was approximately 4 V.

Testing is usually conducted under DC conditions because the transients (as in Figs. 4.1(a) and (c)) [2] are detectable above a static threshold above the noise level. As seen in Fig. 4.1(e) [2], AC transients require more complicated instrumentation thresholding techniques. However, IRES can extract the SET signal even when the error response competes with excessive noise or AC signals. IRES allows for the analysis of short-duration transient behavior via time-frequency anal-
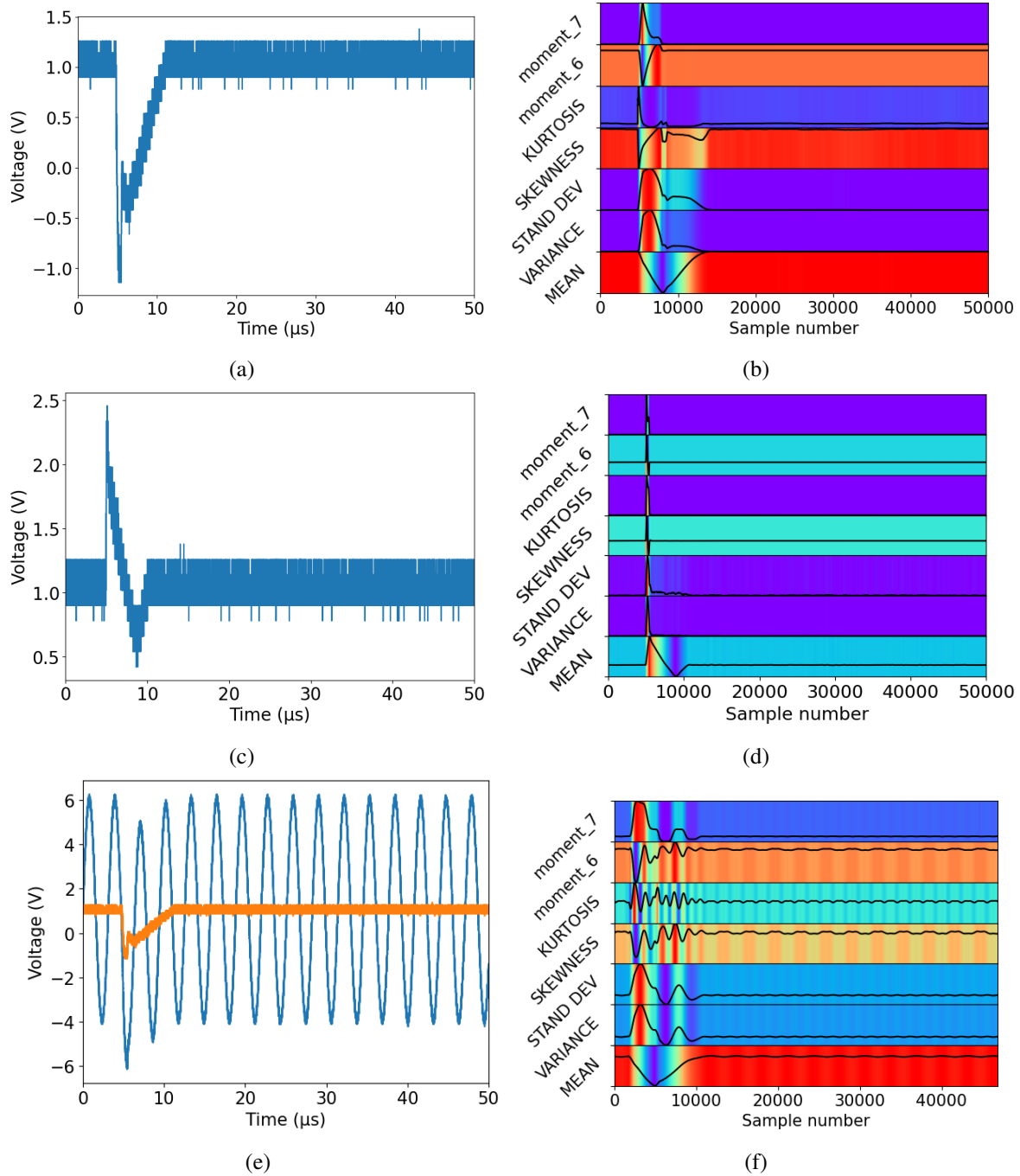
Figure 4.1   Analog SETs in the LM124 following exposure to Xe ions (16 MeV/amu) at LBNL. The incident LET was 49.3 MeV*cm^2/mg. The LM124 was configured in unity gain with a DC input of V$_{in}$= 1 V in (a) and (c) and with a sinusoidal input and a 10 V amplitude in (e). Figs. (b), (d), and (f) are the corresponding IRES spectrograms, including the mean, variance, standard deviation, skewness, kurtosis, and the 6th and 7th moments [2]

ysis [4] and filters out the nominal circuit behavior, thus extracting the error signal. Figs. 4.1(b), (d), and (f) [2] illustrate the IRES spectrograms for the three transients and are constructed using μ, σ, σ^2, κ, γ, and the 6th and 7th moments. The spectrograms are unique to the underlying transient characteristics, as seen by comparing Figs. 4.1(b) and (d) [2], and are readily obtained from DC or sinusoidal signals as seen by comparing Figs. 4.1(b) and (f) [2]. μ represents an AC-filtered version of the original signal. σ and σ^2 are measures of the transient time constants, and κ and γ both signal event transitions. As seen in Fig. 4.1 (f) [2], the steady-state AC sinusoidal waveform has a secondary effect on the calculated moments.

4.2.1 Analysis of oscillation frequency and amplitude shifts

The output signal induced by a SET varies based on the type of integrated circuit (IC), where the strike occurs in the circuit, and the amounts of energy transferred to the semiconductor material. IRES's ability to filter out or reduce the influence that the steady state portion exhibits on the signal, is especially useful for signals that are periodic by design where the identification of SET may not be clearly distinguishable for traditional measurement hardware; for example, with changes in frequency shown in Fig. 4.2 (a) and drops in amplitude shown in Fig.4.2 (c). By setting IRES's Window Size to the signal's period (the time it takes to complete one cycle) the AC portion is dramatically reduced leaving just the DC SET signature. It is important for the window size to be as small as possible to maintain the accuracy of SET features.

Simulations in Python were developed to study IRES's responses to changes in the frequency and amplitude of periodic signals, as well as changes in both frequency and amplitude, as seen in Fig. 4.2 (a), (c), and (e), respectively. For each IRES spectrogram shown in Fig. 4.2 (b),(d), and (f), the window size was set to the steady-state period of the waveform in this case 3311, and with a stride of 2. In all three scenarios, the steady-state oscillation element of the signal was removed, and a DC average was computed for each statistical moment. By separating the frequency and amplitude, the signal's characteristics can be better understood as to how different moments affect the impact of IRES's ability to analyze signals experiencing an ASET. Fig. 4.2 (b) effectively

27
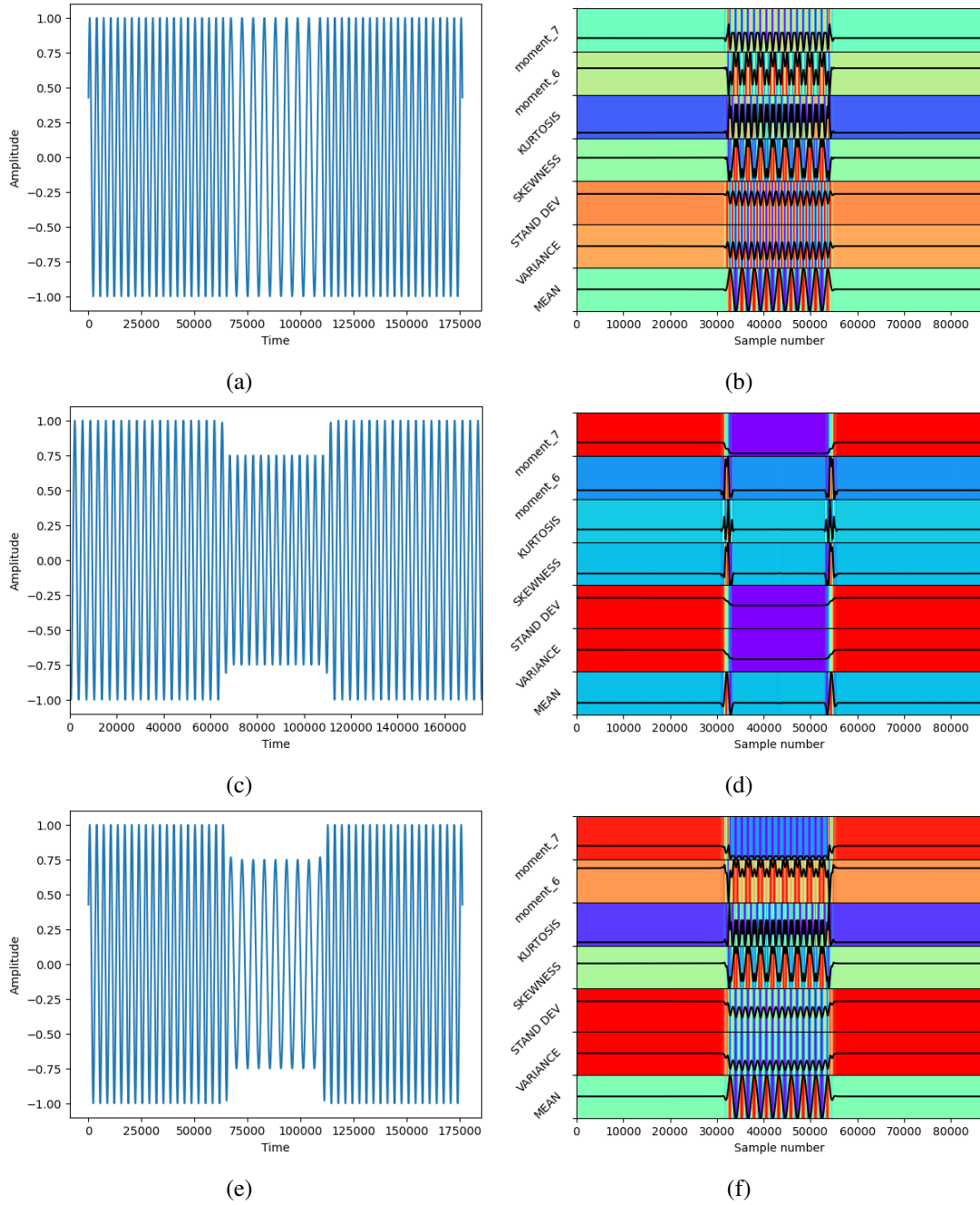
Figure 4.2 Figs. (a) change in frequency, (c) change in amplitude, and (e) change in both frequency and amplitude are examples of ASETs in an oscillating signal. Figs. (b), (d), and (f) are the corresponding IRES spectrograms, including the mean, variance, standard deviation, skewness, kurtosis, and the 6th and 7th moments

28

demonstrates how IRES possesses the capability to detect changes in frequency. This is achieved by optimizing the window to the steady-state period, which allows any frequency changes present in the signal to be amplified as the window moves across the periodic signal. Additionally, Fig. 4.2 (d) showcases the ability of IRES to detect changes in amplitude. Here, all sinusoidal aspects are removed from the signal and only the DC portion remains. Fig.4.2 (f) provides insight into changes in both frequency and amplitude are applied to the periodic signal. The mean, skewness, and kurtosis moments from Fig.4.2 (b), where frequency plays the largest role, exhibit similar statistical features to those observed in Fig.4.2 (f). Similarly, the standard deviation, variance, and 7th moments from Fig.4.2 (d), where the amplitude is the key factor, also have similar statistical features to those observed in Fig.4.2 (f).

4.2.2 Analysis of Dropped Pulses, Shortened Pulses, or Phase Shifts

Pulse Width Modulation (PWM) is a technique used in electronics and communication systems to control the amount of power delivered to a device or component. PWM works by rapidly switching a power source on and off at a fixed frequency while varying the ratio of the on-time to the off-time. The duration of time that the power source is switched on during each cycle is called the pulse width, and it determines the average power delivered to the load. By adjusting the pulse width, the effective voltage or power delivered to the load can be controlled. ASETs can induce changes to the signal's pulse width in terms of a dropped pulse Fig. 4.3 (a), Shortened Pulses Fig. 4.3 (c), or Phase Shifts Fig. 4.3 (e). Using Python to simulate the three different effects so we could observe IRES's responses. For each IRES spectrogram shown in Fig. 4.3 (b),(d), and (f), the window size was set to the period of the waveform in this case 10, and with a stride of 1.

For the dropped pulse Fig. 4.3 (b) and shortened plus Fig. 4.3 (d) IRES was able to identify the ASET anomaly but the pulse width duration is lost for the shortened pulse. One way to correct this loss in the pulse width duration would be to extract the anomaly and perform IRES a second time with a smaller window. For signals that experience a phase shift like Fig. 4.3 (e) where the blue signal is the normal signal and the orange signal contains a phase shift around time forty-five.
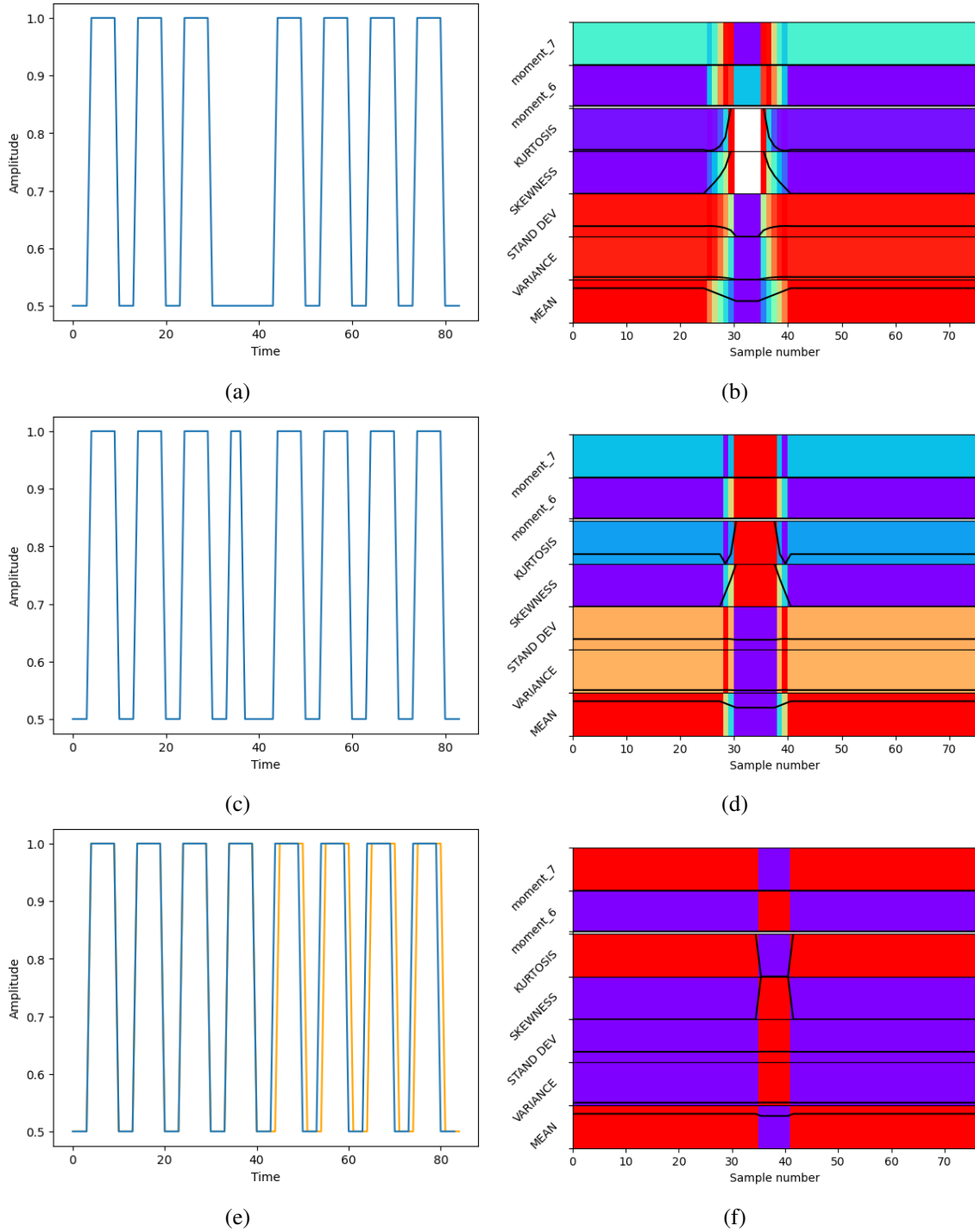
Figure 4.3   Figs. (a) plus drop, (c) shortened plus, and (e) phase shift are examples of ASETs in a PWM signal. Figs. (b), (d), and (f) are the corresponding IRES spectrograms, including the mean, variance, standard deviation, skewness, kurtosis, and the 6th and 7th moments

IRES produces a unique binary transition in all seven-moment features as shown in Fig. 4.3 (f). Although the IRES spectrogram is able to detect the phase shift, Fig. 4.3 (f) could be misinterpreted as an anomaly that occurred for only one cycle before returning back to its designed steady-state, which is not true as seen in Fig. 4.3 (e) where the phase shifted signal (in Orange) continues to the end of the signal. It is important to note, these simulations are of ideal signal waveform conditions and ASET effects, and while useful for understanding IRES abilities for detection further testing is needed for validation.

4.3 IRES for Digital Signals

4.3.1 Deterministic Digital Signals

An 8-bit software DAC and a fault injection tool were developed using Python to accept a discrete-time sequence of 8-bit digital data and convert it to an analog signal for analysis with the IRES module. Fig. 4.4(a) [2] illustrates the 8-bit decimal code with an applied ramp function (counting from 0x00 to 0xFF). Faults (SEUs) were injected by randomly selecting one of eight bits during a random sample out of signal. The SEUs can be seen as positive or negative spikes in the digital ramp signal, having different amplitudes based on which bit was flipped: two are distinct because the SEUs occurred in the most significant bits, whereas one SEU is not visible at scale because it occurred in the least significant bit (LSB). However, when IRES is applied to the digital waveform, shown in Fig. 4.4(b) [2], small changes in κ and γ appear at approximately 150 cycles (sample number), indicating the otherwise undetectable presence of the SEU. The two most significant features for the digital data appear to be κ and γ, as they represent coarse data transitions. The window size for the IRES spectrogram was set to five-time steps with a stride of 1 step. The changing colors represent the normalized values ranging from 0 (purple) to 1 (red). Note that the IRES algorithm does not require a golden sample of the unperturbed data sequence as it establishes probabilities of upset based on prior functionality. Although a DAC with an applied ramp function was used to illustrate the implementation of IRES with binary (base-2) signals, the technique can be applied to any digital code as long as the window is larger than the number of

31
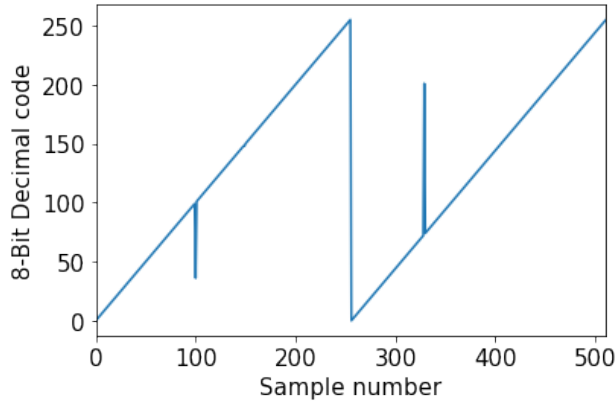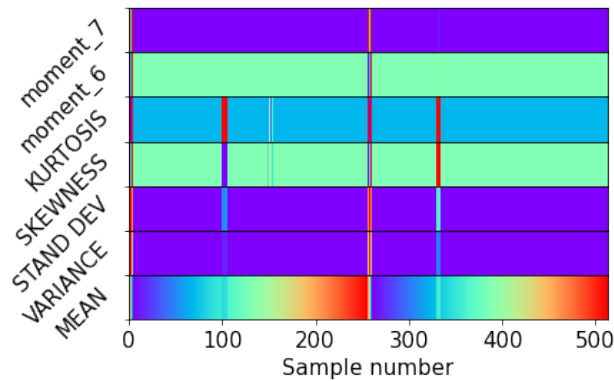
Figure 4.4   (a) SEUs in the software DAC with an applied ramp function and (b) associated IRES spectrogram. Two periods of an 8-bit ramp function are visualized with three SEUs injected in random bit locations. Two SEUs are visible in (a) samples 100 and 325. However, small changes in the skewness and kurtosis indicate the presence of an otherwise undetectable SEU in sample 150. The changing colors represent the normalized values ranging from 0 (purple) to 1 (red) [2]

bits required to represent the base-2 numbers.

4.3.2   Stochastic Digital Signals

Signals with low entropy (such as a ramp function or other deterministic digital data) are straightforward to analyze; however stochastic data with high entropy present a challenge for the technique. When a signal is stochastic, like in digital communication signals, and has a high entropy factor, the IRES methodology loses its effectiveness. One way of detecting SEUs in digital
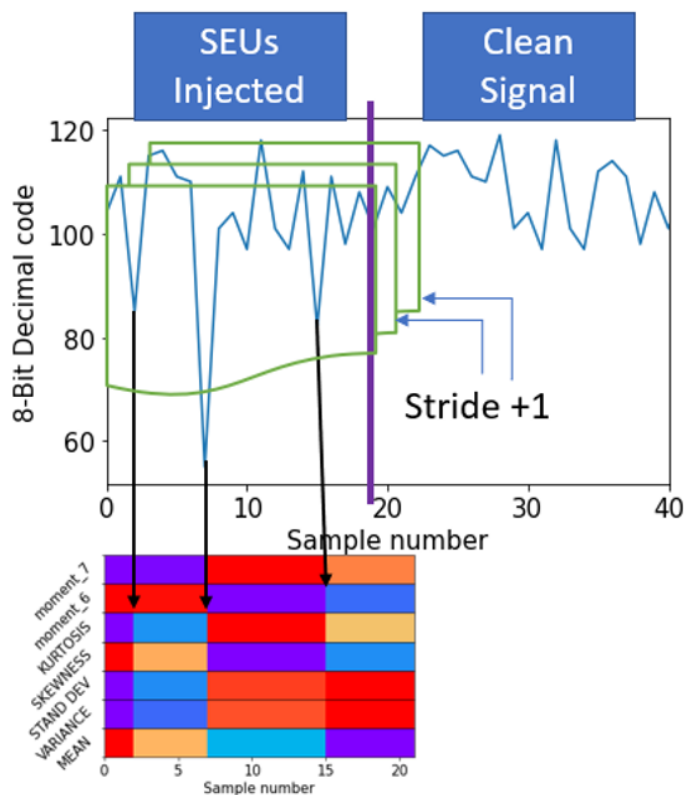
Figure 4.5   (a) SEUs in the software DAC with an applied stochastic digital signal and (b) associated IRES spectrograms. Changes in the mean, variance, standard deviation, skewness and kurtosis indicate the presence of SEUs. The changing colors represent the location of the SEUs

stochastic signals could be through double transmission. By having a double transmission IRES has the ability to compare the two signal's probability distributions functions and find the bits that were flips accrued. As shown in Fig. 4.5 is an example of how IRES was used to compare two transmitted signals. Where you have SEU injected to the left of the purple line and the right a clean signal. The green boxes represent the window size, showing a stride of 1. By having the window size contain all of the first transmission (left of the purple line), IRES can compare the two signal PMFs and find the accrued error using temporally or spatially redundant information, but further work is needed for validation.

4.4   IRES Noise Sensitivity

The IRES window filter is naturally robust to noisy signals as the method extracts transient phenomena based on probabilities. Therefore, a comparison was conducted between a typical thresholding technique (*a priori* determination of signal boundaries, typically based on maximum and minimum levels of acceptable voltage/current) and the IRES method. First, the PLL dataset, including 100,000 transient measurements induced by the TPA laser at NRL, was used to evaluate the sensitivity of IRES with varying window settings and under varying noise constraints. These measured data include ten samples for each location where a SET was injected. These data were augmented by adding artificial random White Gaussian Noise (WGN) to the original waveform data, resulting in SNR values ranging from 0 dB to 13.01 dB. The SNR was calculated by (4.1) where μ is the mean of the expected signal power of the raw data, and σ is the standard deviation of the WGN. To convert SNR to decibels, equation (4.2) is used. The ten unique signals (corresponding to identical locations in the PLL) were each evaluated with a different WGN profile at the same SNR value.

$$SNR = \frac{\mu}{\sigma} \tag{4.1}$$

$$SNR_{dB} = 10log_{10}(SNR) \tag{4.2}$$

Each augmented, noisy waveform consists of 500 timesteps. First, a baseline threshold method was defined; in this case, μ and σ of 100 random waveforms were measured. Next, SETs were defined if any point within a sample fell outside of 3 standard deviations from the mean. This process was repeated for all SNR values.

Additionally, each waveform was transformed using window IRES filters with varying window sizes (ranging from 10% of the time steps to 90% of the time steps) and a fixed stride of 10%. Similar to the baseline amplitude thresholding method, the sensitivity of the individual moments to WGN was evaluated by defining a SET when any point within a sample fell outside of 3 stan-

34
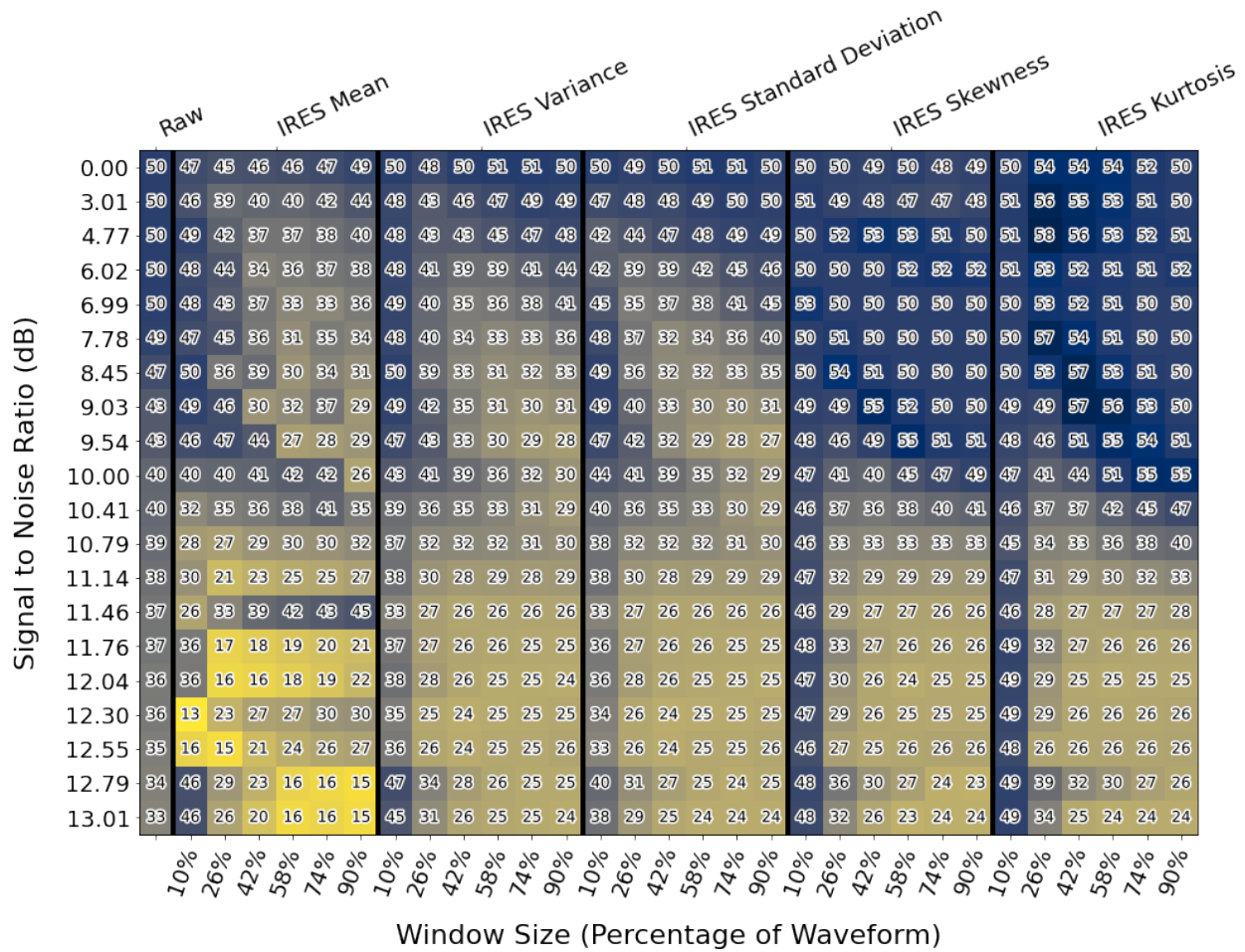
Figure 4.6 Comparison of error thresholding a raw waveform against IRES-generated moments with different window filter sizes. The Y axis represents the SNR, and the bottom X axis portion represents the window size of the IRES filter (in units % of timesteps). The top X axis portion indicates the waveform or time-sequenced moment that was evaluated, separated by the vertical lines [2]

dard deviations from the mean of the moment under study. This process was repeated for all SNR values. The % error was used to compare the results and is determined by (4.3). True positive (TP) represents the number of times a waveform was correctly identified as containing a SET; true negative (TN) represents the number of correctly identified waveforms without a SET; false positive (FP) represents the number of incorrectly identified transients; false negative (FN) represents the number of waveforms incorrectly identified as unperturbed. Note that this process was conducted to examine the sensitivity of each IRES-generated moment to the transient signal and is not

intended to suggest a SET detection process. An IRES-inspired SET detection process will likely involve a combination of moments and ML-based classification.

$$Error = \frac{FN + FP}{TN + TP + FN + FP} \qquad (4.3)$$

Fig. 4.6 [2] shows the % error of a chosen threshold metric (*i.e.*, the original, raw waveform vs. various IRES-generated moments) with respect to window size and SNR. The color corresponds to the error value of each cell. First, the baseline thresholding technique resulted in a minimum error of 31% for an SNR of 13 dB. The method cannot tolerate high levels of noise without defining new metrics. Moreover, transients that exist within the noise boundaries are not detectable. The first and second moments outperform the baseline technique, with μ as perhaps the most reliable single metric for identifying the presence of a transient. The lowest error rate is observed at a window size of 26%; however, larger window sizes improve performance for critically low SNR values. In other words, while small window sizes can be useful for detecting fast transients, calculations will be more sensitive to noise when compared to large window sizes. The third moments and higher are susceptible to noise and cannot be used for transient thresholding except in cases with large SNR values. The % error generally increases with decreasing SNR for all moments, though the SNR value at which the % error saturates increases with increasing moments. There are trade offs in accuracy and precision when implementing the IRES window filter. For example, large window sizes improve tolerance to noise at the sacrifice of precision, whereas smaller window sizes improve accuracy while less effective in filtering noise.

While Fig. 4.7 [2] is intended to show the sensitivity of a single IRES-generated moment to noise and various filter settings, IRES is most beneficial because several time-sequenced moments are generated simultaneously. In this case, an algorithm is required to leverage more than one moment for thresholding an event detector. Nevertheless, the transient nature of the moments can help develop a more complete understanding of the transient phenomena, and be used to build a new definition of a transient threshold or be used in ML applications and classification models such as [5].

36
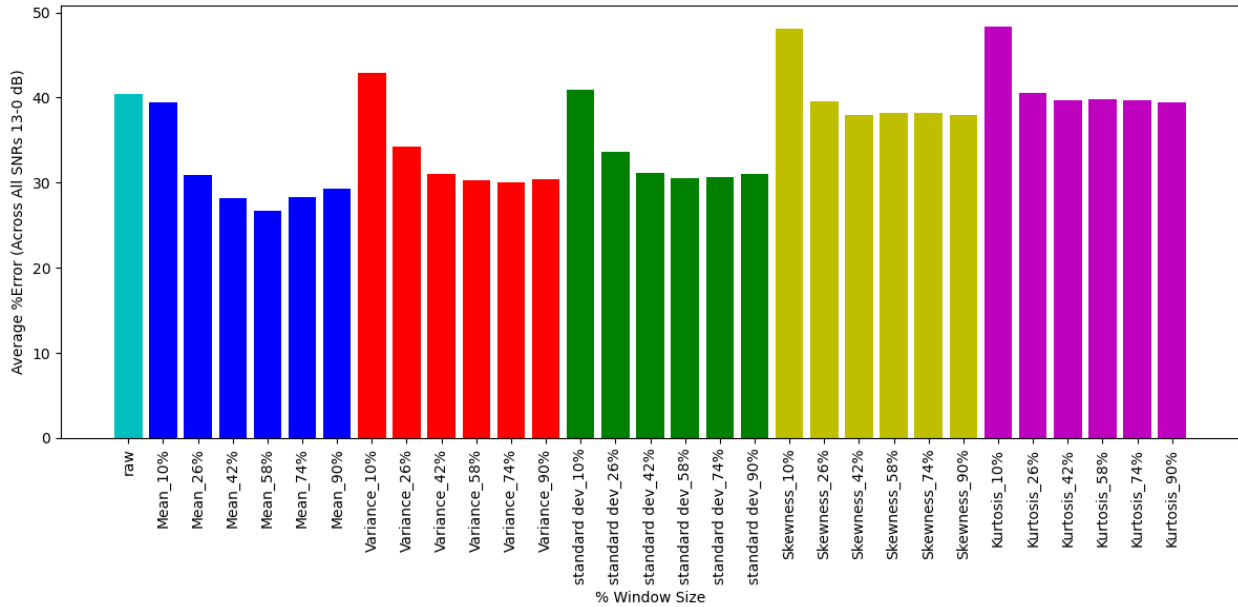
Figure 4.7 Comparison of error thresholding a raw waveform against IRES-generated moments with different window filter sizes. The Y-axis represents the average % error for all SNR values, and the bottom X-axis represents the window size of the IRES filter for each moment (in units % of timesteps)

In addition, IRES window filters may be applied in sequence. Fig. 4.8(a) [2] shows an example analog SET measured at the output of the LM124 following exposure to Xe ions (16 MeV/amu) at LBNL. The incident LET was 49.3 MeV*cm^2/mg. The LM124 was configured in unity gain with a DC input of V$_{in}$= 5 V. Fig. 4.8(b) [2] shows the identical transient with added WGN to reduce the SNR to -17 dB. Two passes of the IRES window filter were applied to these data. IRES$_1$ corresponds to the output of the first IRES window filter, and IRES$_2$ corresponds to the output of the second IRES window filter in sequence. Since the μ of IRES$_1$ was identified as the most informative according to Fig. 4.6 [2], μ from IRES$_1$ was fed back into the IRES algorithm to produce the spectrograms shown in Figs. 4.8 (e) and (f) [2]. A similar process could be conducted using the other moments. The identical spectrograms in Figs. 4.8 (e) and (f) [2] show that IRES is highly effective in removing high levels of noise, allowing for the extraction of the true transient error signals with high accuracy.

37
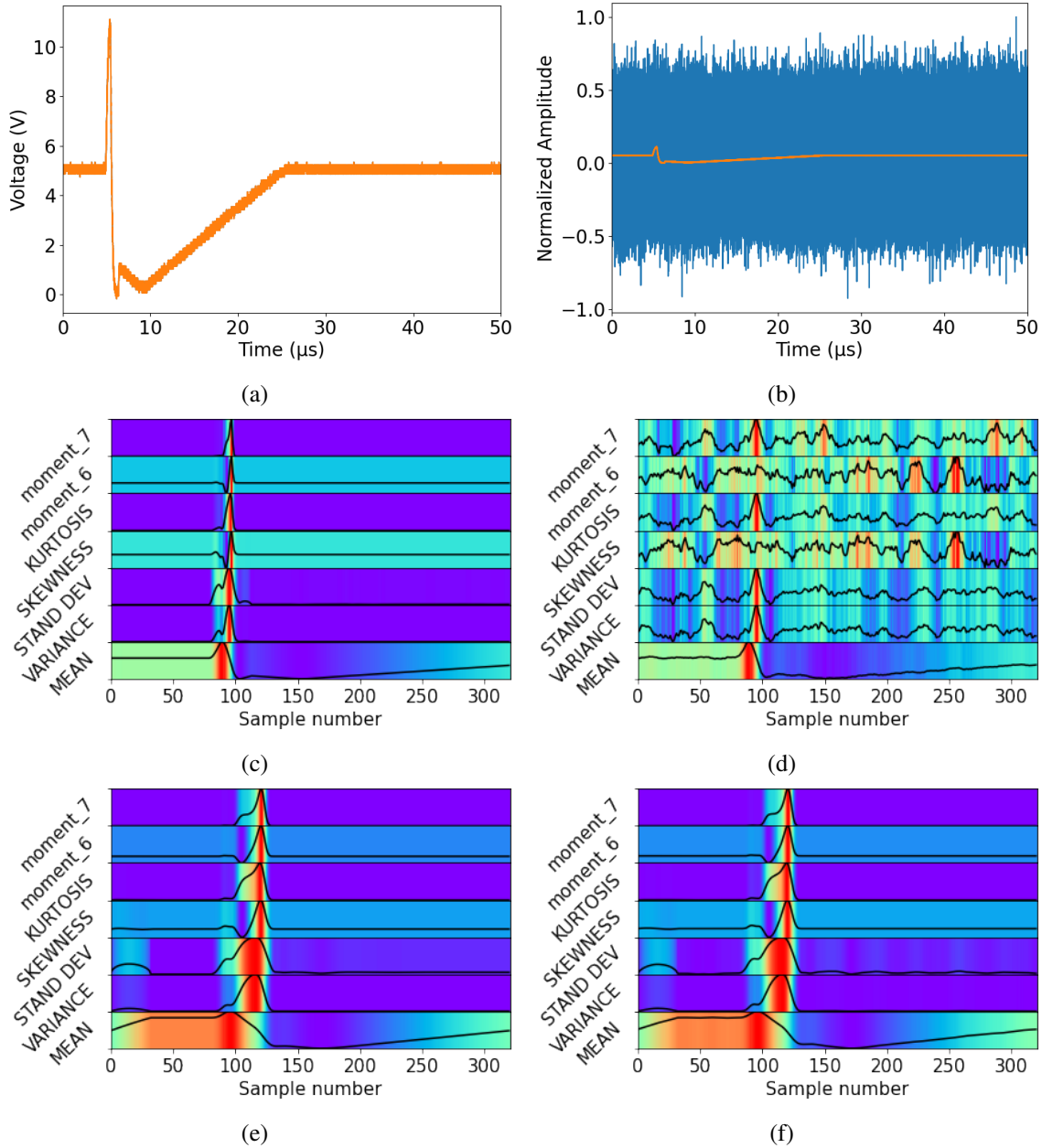
Figure 4.8   Analog SETs in the LM124 following exposure to Xe ions (16 MeV/amu) at LBNL. The incident LET was 49.3 MeV*cm^2/mg. (a) The LM124 was configured in unity gain with a DC input of V$_{in}$= 5 V. (b) The LM124 was configured in unity gain with a DC input of V$_{in}$= 5 V with random WGN added to the transient for an SNR of -17 dB. (c) and (d) are the corresponding spectrograms following one application of the IRES filter (IRES$_1$), while (e) and (f) are the corresponding spectrograms following two sequential applications of the IRES filter (IRES$_2$). Both IRES$_1$ and IRES$_2$ spectrograms include the mean, variance, standard deviation, skewness, kurtosis, and the 6th and 7th moments [2]

4.5 Summary

Measured data shows that the IRES window filter enhances transient analysis by eliminating all steady-state signatures, including continuous noise, and extracts transient behaviors by amplifying shifts in statistical moments. IRES is highly effective in extracting transients within AC waveforms, such as clock signals, without requiring prior signal transformations. Also, by setting the Window Size to the period of a periodic signal, the AC portion gets canceled out, leaving just the DC Signal. The fault injection experiments on an 8-bit digital-to-analog converter (DAC) illustrate the ability to detect single event upsets (SEUs) in a digital sequence. The most notable indicators for an SEU in a deterministic signal are in the skewness and kurtosis moments. Finally, the performance of the IRES filter in noisy environments shows that a single IRES filter can reduce the signal-to-noise ratio (SNR) requirement for detection by over 10 dB, and sequential IRES filters can improve the response by over 20 dB when compared to traditional threshold triggers. Additionally, while threshold triggers require a positive-valued SNR, IRES is shown effective even with SNR values as low as -17 dB, detecting anomalies in high noise environments without requiring multi-sampling.

CHAPTER 5

FUTURE WORK

In future work, an important direction is the implementation of the Ionizing Radiation Effects Spectroscopy (IRES) dynamic statistical trigger mentioned in Chapter 3 for in-situ analysis using instrumentation hardware such as an oscilloscope. Currently, IRES method has been only used for automating post-processing data to extract transient behavior for analysis. However, by integrating this dynamic statistical trigger into the instrumentation would enable real-time monitoring and detection of transient events. Also, This would provide valuable insights into the behavior of the circuit during operation and allow for immediate response or mitigation strategies in the presence of Single Event Effects (SEE). The implementation of IRES's dynamic trigger in the instrumentation would enhance the efficiency and effectiveness of radiation testing, enabling more accurate and timely identification of SETs and ASETs, ultimately leading to improved device reliability and performance in radiation environments.

CHAPTER 6

CONCLUSION

The harsh conditions of space pose significant challenges for electronic systems due to radiation from solar emissions and Galactic Cosmic Rays (GCR). This ionizing radiation can cause Single-Event Transients (SETs) in electronic systems operating in space. Before a mission, individual electronic components undergo accelerated radiation testing to understand radiation's effects on microelectronics and effectively implement radiation-hardening-by-design (RHBD) technique in their systems. With the increased commercialization of space, there is a higher demand for faster and more efficient ground-based radiation testing facilities. Commercial off-the-shelf (COTS) components and systems-on-chip (SOC) often require extra time. Automation techniques for radiation testing and analysis have become crucial to meet the growing constraints and demands for available time at heavy ion facilities. This work analyzes two areas for improvement when it comes to radiation testing: 1) improving the fidelity of detection of single event effects in arbitrary signals and 2) eliminating added environmental noise.

This approach presents Ionizing Radiation Effects Spectroscopy (IRES) as a powerful technique that enables the characterization of ionizing radiation effects in devices and systems, by extracting waveform features and analyzing statistical profiles in arbitrary signals. IRES allows for a thorough assessment of transient behavior while eliminating added environmental noise. The proposed IRES window filter is an exceptionally effective tool for filtering unwanted noise. It accomplishes this by utilizing a unique approach that identifies transient events based on a statistical window analysis technique. In order to assess its efficacy, a comparison between the IRES filter and a more traditional thresholding technique that relies on pre-determined voltage and current levels to identify signals is provided. The evaluation resulted in guidelines for applying IRES un-

der a variety of noise conditions. Findings indicate that the IRES filter significantly outperformed the threshold triggers by reducing the signal-to-noise ratio requirement for detection by more than 10 dB. Moreover, when sequential IRES filters were applied, the response was further improved by over 20 dB in noisy environments. Unlike threshold triggers, the IRES filter remained effective even in high-noise environments with SNR values as low as -17 dB, without requiring multi-sampling.

IRES is a tool that can detect SET signatures in various signals, including digital data busses, analog DC and sinusoidal waveforms, and RF signals, without the need for an arbitrary error threshold. The IRES window filter is useful for transient analysis as it removes steady-state signatures like continuous noise and amplifies shifts in statistical moments to extract transient behaviors. It can even extract transients within AC waveforms like clock signals without any signal transformations. By adjusting the Window Size to the period of a periodic signal, IRES can cancel out the AC portion and leave only the DC Signal. In experiments with an 8-bit digital-to-analog converter (DAC), IRES detected single event upsets (SEUs) in a digital sequence. The skewness and kurtosis moments were significant indicators for an SEU in a deterministic signal.

This work presents a statistical window analysis technique for improving the efficiency of data collection during radiation testing. IRES may remove the need for complex triggering mechanisms on instrumentation and does not require *a-priori* knowledge of transient characteristics. This can lead to better implementation of RHBD technique in systems and chip development.

REFERENCES

[1] E. Mathieu and M. Roser, "Space exploration and satellites," Our World in Data, 2022, https://ourworldindata.org/grapher/yearly-number-of-objects-launched-into-outer-space?time=2000..latest.

[2] J. L. Carpenter, T. N. Peyton, B. R. Dean, S. P. Lawrence, R. D. Young, D. R. Reising, and T. D. Loveless, "Analysis of single event transients in arbitrary waveforms using statistical window analysis," IEEE Transactions on Nuclear Science, vol. 70, no. 4, pp. 478–485, April 2023.

[3] B. Patel, M. Joplin, R. C. Boggs, D. R. Reising, M. W. McCurdy, L. W. Massengill, and T. D. Loveless, "Ionizing Radiation Effects Spectroscopy for Analysis of Total-Ionizing Dose Degradation in RF Circuits," vol. 66, no. 1, pp. 61–68, Jan. 2019.

[4] T. D. Loveless, B. Patel, D. R. Reising, R. Roca, M. Allen, L. W. Massengill, and D. Mc-Morrow, "Ionizing Radiation Effects Spectroscopy for Analysis of Single-Event Transients," vol. 67, no. 1, pp. 99–107, Jan. 2020.

[5] T. D. Loveless, D. R. Reising, J. C. Cancelleri, L. W. Massengill, and D. McMorrow, "Analysis of Single-Event Transients (SETs) Using Machine Learning (ML) and Ionizing Radiation Effects Spectroscopy IRES," vol. 68, no. 8, pp. 1600–1606, Jan. 2021.

[6] "NASA - sources of ionizing radiation in interplanetary space."

[7] J. A. Van Allen, C. E. McIlwain, and G. H. Ludwig, "Radiation observations with satellite 1958 ," Journal of Geophysical Research (1896-1977), vol. 64, no. 3, pp. 271–286, 1959. [Online]. Available: https://agupubs.onlinelibrary.wiley.com/doi/abs/10.1029/JZ064i003p00271

[8] T. D. Loveless, "Hardening Techniques for Analog and Mixed-Signal Circuits," IEEE NSREC Short Course, pp. III.1–III.96, July 2021.

[9] R. Baumann, "Single-event effects in advanced CMOS," IEEE NSREC Short Course, pp. II.1–II.59, July 2005.

[10] P. Dodd and L. Massengill, "Basic mechanisms and modeling of single-event upset in digital microelectronics," IEEE Transactions on Nuclear Science, vol. 50, no. 3, pp. 583–602, June 2003.

[11] L.W.Massengill, "SEU modeling and prediction techniques," IEEE NSREC Short Course, pp. III.1–III.93, July 1993.

[12] S. E. Diehl, J. E. Vinson, B. D. Shafer, and T. M. Mnich, "Considerations for single event immune vlsi logic," IEEE Transactions on Nuclear Science, vol. 30, no. 6, pp. 4501–4507, Dec 1983.

[13] S. E. Diehl-Nagle, J. E. Vinson, and E. L. Peterson, "Single event upset rate predictions for complex logic systems," IEEE Transactions on Nuclear Science, vol. 31, no. 6, pp. 1132–1138, Dec 1984.

[14] A. L. Friedman, B. Lawton, K. R. Hotelling, J. C. Pickel, V. H. Strahan, and K. Loree, "Single event upset in combinatorial and sequential current mode logic," IEEE Transactions on Nuclear Science, vol. 32, no. 6, pp. 4216–4218, Dec 1985.

[15] V. Ferlet-Cavrois, L. W. Massengill, and P. Gouker, "Single event transients in digital cmos—a review," IEEE Transactions on Nuclear Science, vol. 60, no. 3, pp. 1767–1790, June 2013.

[16] F. Sexton, ""Measurement of Single Event Phenomena in Devices and ICs," IEEE NSREC Short Course, pp. III.1–III.55, July 1992.

[17] S. Buchner and D. McMorrow, "Single-event transients in bipolar linear integrated circuits," IEEE Transactions on Nuclear Science, vol. 53, no. 6, pp. 3079–3102, Dec 2006.

[18] L. W. Massengill and P. W. Tuinenga, "Single-event transient pulse propagation in digital cmos," IEEE Transactions on Nuclear Science, vol. 55, no. 6, pp. 2861–2871, Dec 2008.

[19] D. Mavis and P. Eaton, "Soft error rate mitigation techniques for modern microcircuits," in 2002 IEEE International Reliability Physics Symposium. Proceedings. 40th Annual (Cat. No.02CH37320), April 2002, pp. 216–225.

[20] S. Buchner and D. McMorrow, "Single-Event Transients in Bipolar Linear Integrated Circuits," vol. 53, no. 6, pp. 3079–3102, Dec. 2006.

[21] J. Howard, M. Carts, K. LaBel, J. Forney, and T. Irwin, "Single event effects testing of the linfinity sg1525a pulse width modulator controller," in 2003 IEEE Radiation Effects Data Workshop, July 2003, pp. 133–140.

[22] W. Chen, V. Pouget, H. Barnaby, J. Cressler, G. Niu, P. Fouillat, Y. Deval, and D. Lewis, "Investigation of single-event transients in voltage-controlled oscillators," IEEE Transactions on Nuclear Science, vol. 50, no. 6, pp. 2081–2087, Dec 2003.

[23] F. Bezerra and V. Pouget, "FACILITIES AND METHODS FOR RADIATION TESTING," IEEE NSREC Short Course, pp. IV–II.1–IV–II.35, July 2014.

[24] R. Mangeret, "Radiation hardness assurance: how well assured do we need to be?" IEEE NSREC Short Course, pp. II.1–II.64, July 2018.

[25] D. R. Reising, M. A. Temple, and J. A. Jackson, "Authorized and Rogue Device Discrimination Using Dimensionally Reduced RF-DNA Fingerprints," vol. 10, no. 6, pp. 1180–1192, June 2015.

[26] L. Xiao, L. Greenstein, N. Mandayam, and W. Trappe, "Fingerprints in the Ether: Using the Physical Layer for Wireless Authentication," in 2007 IEEE International Conference on Communications, Aug. 2007, pp. 4646–4651.

[27] B. Kroon, S. Bergin, I. O. Kennedy, and G. O'Mahony Zamora, "Steady State RF Fingerprinting for Identity Verification: One Class Classifier versus Customized Ensemble," in Artificial Intelligence and Cognitive Science, L. Coyle and J. Freyne, Eds. Berlin, Germany: Springer, 2010, pp. 198–206.

[28] C. K. Dubendorfer, B. W. Ramsey, and M. A. Temple, "An RF-DNA verification process for ZigBee networks," in MILCOM 2012 - 2012 IEEE Military Communications Conference, Oct. 2012, pp. 1–6.

[29] D. R. Reising and M. A. Temple, "WiMAX mobile subscriber verification using Gabor-based RF-DNA fingerprints," in 2012 IEEE International Conference on Communications (ICC), June 2012, pp. 1005–1010.

[30] D. R. Reising, "Exploitation of RF-DNA for Device Classification and Verification Using GRLVQI Processing," Ph.D. dissertation, Air Force Institute of Technology, Dec. 2012.

[31] W. Wang, Z. Sun, S. Piao, B. Zhu, and K. Ren, "Wireless physical-layer identification: Modeling and validation," vol. 11, no. 9, pp. 2091–2106, Sep. 2016.

[32] G. Baldini, R. Giuliani, and G. Steri, "Physical Layer Authentication and Identification of Wireless Devices Using the Synchrosqueezing Transform," Applied Sciences, vol. 8, p. 2167, Nov. 2018.

[33] Q. Tian, Y. Lin, X. Guo, J. Wen, Y. Fang, J. Rodriguez, and S. Mumtaz, "New Security Mechanisms of High-Reliability IoT Communication Based on Radio Frequency Fingerprint," vol. 6, no. 5, pp. 7980–7987, Oct. 2019.

[34] F. Kandah, J. Cancelleri, D. Reising, A. Altarawneh, and A. Skjellum, "A Hardware-Software Codesign Approach to Identity, Trust, and Resilience for IoT/CPS at Scale," in Proc. Int. Conf. Internet Things (iThings), July 2019, pp. 1125–1134.

[35] G. Baldini, R. Giuliani, and C. Gentile, "An assessment of the impact of IQ imbalances on the physical layer authentication of IoT wireless devices," in 2019 Global IoT Summit (GIoTS), June 2019, pp. 1–6.

[36] D. R. Reising, M. A. Temple, and M. J. Mendenhall, "Improving Intra-Cellular Security Using Air Monitoring with RF Fingerprints," in 2010 IEEE Wireless Communication and Networking Conference, Apr. 2010, pp. 888–893.

[37] D. Reising, J. Cancelleri, T. D. Loveless, F. Kandah, and A. Skjellum, "Radio Identity Verification-Based IoT Security Using RF-DNA Fingerprints and SVM," vol. 8, no. 10, pp. 8356–8371, May 2021.

[38] J. F. Ziegler, M. D. Ziegler, and J. P. Biersack, "SRIM - The stopping and range of ions in matter (2010)," Nuclear Instruments and Methods in Physics Research B, vol. 268, no. 11-12, pp. 1818–1823, Jun. 2010.

[39] T. D. Loveless, L. W. Massengill, W. T. Holman, B. L. Bhuva, D. McMorrow, and J. H. Warner, "A Generalized Linear Model for Single Event Transient Propagation in Phase-Locked Loops," vol. 57, no. 5, pp. 2933–2947, Oct. 2010.

[40] D. McMorrow, W. T. Lotshaw, J. S. Melinger, S. Buchner, and R. L. Pease, "Subbandgap laser-induced single event effects: carrier generation via two-photon absorption," vol. 49, no. 6, pp. 3002–3008, Dec. 2002.

[41] D. McMorrow, W. T. Lotshaw, J. S. Melinger, S. Buchner, Y. Boulghassoul, L. W. Massengill, and R. L. Pease, "Three-dimensional mapping of single-event effects using two photon absorption," vol. 50, no. 6, pp. 2199–2207, Dec. 2003.

[42] E. W. V. Stryland, H. Vanherzeele, M. A. Woodall, M. J. Soileau, A. L. Smirl, S. Guha, and T. F. Boggess, "Two Photon Absorption, Nonlinear Refraction, And Optical Limiting In Semiconductors," Optical Engineering, vol. 24, no. 4, pp. 613 – 623, Aug. 1985.

[43] T. Boggess, K. Bohnert, K. Mansour, S. Moss, I. Boyd, and A. Smirl, "Simultaneous measurement of the two-photon coefficient and free-carrier cross section above the bandgap of crystalline silicon," vol. 22, no. 2, pp. 360–368, Feb. 1986.

[44] A. Khachatrian, N. J. . Roche, D. McMorrow, J. H. Warner, S. P. Buchner, and J. S. Melinger, "A Dosimetry Methodology for Two-Photon Absorption Induced Single-Event Effects Measurements," vol. 61, no. 6, pp. 3416–3423, Dec. 2014.

VITA

James Lynn Carpenter II was born in Chattanooga, Tennessee, to his parents James and Tina. He is the youngest of two children, with one older sister. He received his Bachelor of Science degree in Electrical and Electronics Engineering in 2020 from the University of Tennessee at Chattanooga. After graduation, he started his master's the following fall semester, 2020, at the University of Tennessee at Chattanooga. After graduating, James accepted a graduate offer from Indiana University to pursue a doctor of philosophy degree. His research focuses on Radiation Effects, Deep Learning, and the reliability of Microelectronics in Space.